Non-invasive temporal interference electrical stimulation of the human hippocampus

Ines R. Violante[1*], Ketevan Alania[2,3], Antonino M. Cassarà[4], Esra Neufeld[4], Emma Acerbo[5], Romain Carron[5,6], Adam Williamson[5,7], Danielle L. Kurtin[1], Edward Rhodes[2,3], Adam Hampshire[8], Niels Kuster[4], Edward S. Boyden[9,10], Alvaro Pascual-Leone[11,12] and Nir Grossman[2,3*]

[1]School of Psychology, Faculty of Health and Medical Sciences, University of Surrey, Guildford GU2 7XH, UK.

[2]Department of Brain Sciences, Imperial College London, London W12 0HS, UK.

[3]UK Dementia Research Institute (UK DRI) at Imperial College London, London, W12 0NN, UK.

[4]Foundation for Research on Information Technologies in Society (IT'IS), 8004 Zurich, Switzerland.

[5]Aix-Marseille Université, Inserm, Institut de Neurosciences des Systèmes (INS) UMR_S 1106, Marseille, France.

[6]Department of Functional and Stereotactic Neurosurgery, Timone University Hospital, Marseille, France.

[7]Center for Bioelectronic Medicine, Department of Medicine, Solna, Karolinska Institutet, Stockholm, Sweden

[8]The Computational, Cognitive and Clinical Neuroimaging Laboratory, Imperial College London SW7 2BU, UK.

[9]Departments of Brain and Cognitive Sciences, Media Arts and Sciences, and Biological Engineering, McGovern and Koch Institutes, MIT, Cambridge, MA 02139, USA.

[10]Howard Hughes Medical Institute, Cambridge, MA 02138, USA.

[11]Hinda and Arthur Marcus Institute for Aging Research and Deanna and Sidney Wolk Center for Memory Health, Hebrew SeniorLife, Boston, MA 02131, USA

[12]Department of Neurology, Harvard Medical School, Boston, MA 02115, USA

*Correspondence: ines.violante@surrey.ac.uk (I.R.V.), nirg@imperial.ac.uk (N.G.)

SUMMARY

Temporal interference (TI) is a strategy for non-invasive steerable stimulation of neurons deep in the brain using multiple kHz-range electric fields with a difference frequency within the range of neural activity. Here we report the validation of the TI stimulation concept in humans. We used electric field modelling and measurements in a human cadaver to verify that the locus of the transcranial TI stimulation can be steerably focused in the hippocampus with minimal exposure to the overlying cortex. We then used functional magnetic resonance imaging (fMRI) to investigate physiological changes in hippocampal activity during stimulation. TI modulated hippocampal activity during the performance of an episodic memory task. In an additional study, prolonged exposure to TI stimulation improved episodic memory accuracy in a healthy human cohort. Our findings demonstrate the utility of TI stimulation by non-invasively modulating hippocampal neural activity in humans.

INTRODUCTION

A multitude of brain disorders have debilitating impacts on quality of life, with neurological conditions being increasingly recognised as major causes of death and disability worldwide, accounting for approximately 30% of the global burden of disease (GBD) (Silberberg et al., 2015). The majority of patients with brain disorders are unamenable to any form of treatment when pharmacological drugs are ineffective or limited in effectiveness or by toxicities (Gravitz, 2011; O'Brien et al., 2014). As the world population grows and ages, there is an unparalleled need for the development of treatment strategies that can alleviate this burden. Physical means of brain stimulation, known as 'neuromodulation', represent a tenable, non-pharmacological, treatment strategy that acts through direct control of the aberrant neural activity underpinning the diseases or their symptomatic manifestation. Invasive electrical deep brain stimulation (DBS) via implanted electrodes has been used around the world to treat patients with severe movement disorders, such as Parkinson's disease (Benabid et al., 2009), and affective disorders, such as obsessive–compulsive disorder (Greenberg et al., 2010). In addition, DBS is being investigated as a treatment for other conditions, such as depression (Mayberg et al., 2005; Scangos et al., 2021) and Alzheimer's disease (Kuhn et al., 2015; Lozano et al., 2016). However, the risk associated with inserting electrodes into the brain makes exploration of different brain targets difficult and limits potential therapeutic impact (Benabid et al., 2009; Pikov, 2015).

Non-invasive stimulation methods, such as transcranial magnetic stimulation (TMS) and transcranial electrical stimulation (TES) have been used in many human clinical investigations (Hallett, 2007; Nitsche and Paulus, 2011). In the USA, several devices and protocols for TMS are cleared by the Food and Drug Administration (FDA) for various

indications (Lefaucheur et al., 2014). However, the ability of TMS or TES to directly stimulate deeper brain structures is achieved at the expense of inducing stronger stimulation of the overlying cortical areas, resulting in unanticipated side effects that can approach the limits of safety guidelines (Deng et al., 2013).

We recently reported a strategy for sculpting electrical fields to enable focused yet non-invasive neural stimulation at depth (Grossman et al., 2017). By delivering multiple electric fields to the brain at slightly different frequencies within the kHz range—which are themselves higher than the frequency range of endogenous neural activity, but for which the difference frequency is sufficiently low to drive neural activity—neurons can be electrically activated at a selected focus without driving neighbouring or overlying regions. We call this strategy temporal interference (TI) stimulation, since the interference of multiple electric fields is what enables its focality: neural stimulation will occur at the targeted region, for which the amplitude of the electric field envelope modulation, at the difference frequency, is of greater magnitude. **Figure 1A** shows a schematic of the TI stimulation concept. In contrast to traditional electrical stimulation, the stimulus location (i.e., the peak envelope modulation) depends on the relative amplitude and orientation of the applied currents. Thus, by varying the relative current strengths and locations of the electrode pairs, the three-dimensional (3D) region exposed to low frequency modulation can be steered. We validated the TI stimulation concept in the mouse brain both electrophysiologically and by imaging *c-fos* as a biochemical marker of neural activation. We demonstrated that TI stimulation can selectively mediate activation in a deep neural structure, i.e., the hippocampus, without activating the overlying cortical neurons, and steerably target brain regions without physically moving the electrodes (Grossman et al., 2017).

Here, we aim to test the translation of these results to humans by investigating the application of TI to the human hippocampus. We first focused on validating the locus of TI stimulation using computational modelling and cadaver measurements. We followed this by performing simultaneous TI and functional magnetic resonance imaging (fMRI) experiments designed to explore physiological changes in brain activity in response to stimulation, and provide evidence for target engagement. Finally, we tested the behavioural impact of delivering TI stimulation to the hippocampus in healthy human subjects. We demonstrate the safety and tolerability of TI in humans, the ability to focally target the stimulation locus to the human hippocampus, and the capacity to modulate hippocampal activity and behavioural performance.

RESULTS

Validation of Hippocampal Targeting Using Computational Modelling and Cadaver Measurements

We first examined whether the locus of TI stimulation can be localised to the hippocampus with minimal exposure of the overlying cortex by computing the distribution of the electric fields in a detailed anatomical model and experimental measurements in a human cadaver. The predicted locus of TI stimulation is in the region with the largest field envelope modulation amplitude (Grossman et al., 2017), in contrast to conventional alternating current (AC) stimulation for which the locus is the region with the largest absolute field amplitude (Antal and Paulus, 2013). We positioned two pairs of electrodes on the scalp in a trapezoidal configuration that targets the left hippocampus. **Figure 1B** shows a schematic of the electrode configuration.

We first computed the field distribution in an established human anatomical model, i.e., the MIDA model (Iacono et al., 2015) that distinguishes a large number of distinct tissue classes derived from high-resolution multi-modal MRI data, and accounts for electrical conductivity anisotropy and neural orientation based on diffusion tensor imaging (DTI) data. We applied two sinusoidal currents at 2.005 kHz and 2 kHz (resulting in a Δf envelope frequency of 5 Hz) and an equal amplitude of 1 mA (current density ~0.45 mA/cm^2), i.e., TI with 1:1 current ratio ('TI 1:1'), **Figure 1Ci**, and computed the fields' envelope modulation amplitude and absolute amplitude along the (DTI-derived) principal fibres axis in regions-of-interest (ROIs) at the left, i.e. stimulated, hippocampus ('Hipp') and the overlying cortical regions, both underneath the stimulation electrodes (anterior, 'Crtx_Ant'; posterior, 'Crtx_Post') and between the stimulation electrodes (middle, 'Crtx_Mid'). **Figure 1Di** shows a schematic of the hippocampal and cortical ROIs relative to the location of the stimulation electrodes. We found that the fields' envelope modulation amplitude in the hippocampus was at least 30% larger than in the overlying cortical regions (Hipp, 0.26±0.04 V/m median±standard deviation (SD); Crtx_Ant, 0.18±0.10 V/m, ~30% smaller than Hipp; Crtx_Mid, 0.12±0.11, ~53% smaller; Crtx_Post, 0.10±0.09 V/m, ~61% smaller), **Figure 1Dii**. In contrast, the fields' absolute amplitude in the hippocampus was smaller than in the overlying cortical region underneath the Ant electrode (Hipp, 0.29±0.04; Crtx_Ant, 0.30±0.17 V/m, ~3% smaller; Crtx_Mid, 0.23±0.11, ~20% larger; Crtx_Post, 0.21±0.13 V/m, ~28% larger), **Figure 1Diii**, see also **Figure S1** for further visualisation of the TI field distribution.

Given the distinctive functional organization along the hippocampal longitudinal axis (Strange et al., 2014), we next explored the relative distribution of the TI electric fields between the Anterior ('Ant'), Middle ('Mid') and Posterior ('Post') regions of the hippocampus, **Figure**

1Ei. We found that the hippocampal regions were exposed to similar envelope modulation amplitudes (relative to the total hippocampal exposure), **Figure 1Eii**. Since the anterior hippocampal region has been explicitly implicated in successful associative encoding (Chua et al., 2007), we explored whether the locus of the TI electric fields can be steered to this region of the hippocampus. By reducing the current amplitude in one electrode pair and increasing the current amplitude in the second electrode pair by the same amount (i.e., keeping the current sum fixed), the stimulation locus can be steered towards the electrode pair with the smaller current amplitude (Grossman et al., 2017). Thus, we reduced the current in the anterior electrode pair *e1-e2* to 0.5 mA (current density ~0.225 mA/cm^2) and increased the amplitude in the posterior electrode pair *e3-e4* to 1.5 mA (current density ~0.675 mA/cm^2), i.e., TI with 1:3 current ratio ('TI 1:3'), **Figure 1Cii**, and repeated the computation of the field envelope modulation amplitude in the hippocampal ROIs. We found that the TI 1:3 stimulation could increase the relative envelope modulation amplitude in the Ant hippocampal region (i.e., Ant region was ~10% larger than Mid region and ~14% larger than the Post region), **Figure 1Eii**.

To experimentally validate that the locus of TI stimulation could indeed be targeted to the hippocampus, we applied the same electrode configuration as in **Figure 1B** and sinusoidal currents as in **Figure 1Ci** to a human cadaver and measured the electrical potential at the stimulated region using intracranial electrodes. **Figure 1F** shows a CT image of the cadaver with the stimulating scalp electrodes (shown in green and orange discs) and the intracranial recording electrodes (left side of the image, see electrodes *a*, *b* and *c*) implanted in the left mesial temporal lobe, perpendicular to the hippocampus long axis. **Figure 1G** shows the distribution of the normalised envelope modulation amplitude (panel i) and absolute amplitude (panel ii) across the measured brain region (boxed region in **Figure 1F**). Consistent with our modelling, we found that the normalised envelope modulation amplitude was largest in the hippocampal region. In this case, the amplitude was ~74% larger in the hippocampus compared to the overlying cortex, **Figure 1Hi** and **Table S1**. The largest electric field's envelope modulation amplitude along the recording electrode *b* between the two stimulation electrodes *e1* and *e2* (i.e., a field direction perpendicular to the hippocampal longitudinal axis) was 0.09 V/m at a depth of 43.5 mm (consistent with the location of the hippocampus (Wicks et al., 2020)). The envelope modulation ratio along electrode *b* was low at the cortex (e.g., ~7% at 12 mm depth) and high near the hippocampus (e.g., ~90% at 50 mm depth), **Figure 1I**. In contrast, the absolute amplitude was largest in the overlying cortical region. In this case, the normalized amplitude was ~52% larger in the cortex compared to the underlying hippocampus, **Figure 1Hii** and **Table S1**. Accordingly, the largest electric field's amplitude along the recording electrode *b* was 0.3 V/m at 12 mm depth. The distribution of the absolute amplitude was similar when we apply two sinusoids at the Δf frequency of 5 Hz, **Figure S2**.

The results from the electric field modelling and human cadaver measurements suggest that the locus of TI stimulation could be steerably localised in the human hippocampal regions with reduced exposure to the overlying cortex.

Probing the Physiological Effect of TI stimulation on Hippocampal Episodic Memory Activity

After establishing that the TI stimulation locus could be focally and steerably targeted to the hippocampus, we aimed to test whether the stimulating fields could modulate hippocampal neural activity. To do so, we performed simultaneous TI-fMRI to measure the effects of TI stimulation on blood-oxygenation-level-dependent (BOLD) signal. We delivered short stimulation periods in a ON/OFF design to minimise build-up while maximising signal-to-noise-ratio to assess physiological responses. Stimulation was delivered while participants performed a hippocampal-dependent paired associative task, known to robustly evoke BOLD signal in the hippocampus (Sperling et al., 2003; Zeineh et al., 2003). The presence of endogenous activity, promoted by a constrained brain state (i.e. memory encoding) should provide a good initial preparation to investigate possible effects of TI, as it is well established that the level of neuronal background activity modulates the stimulus-induced BOLD response, such that identical stimuli delivered under different amounts of neuronal activity can trigger different BOLD responses (Angenstein, 2014; Li et al., 2019).

Twenty healthy participants (mean age 27.1 ± 7.6 SD; 11 female) performed a face-name paired associative task over 9 blocks of encoding and recall while we recorded brain activity. Each block contained 16 unique face-name pairs (total encoding period 32 s) followed by a delay and a recall period, where participants tried to select the correct name of each face out of five options (i.e., one target name, two foil names that were present in the block but associated with a different face, and two distracting names that were not present during the task). After each name selection, participants were asked to rate their choice confidence. **Figure 2A** shows a schematic of the paradigm. Stimulation was applied using the same electrode configuration as in **Figure 1B** across three conditions: 1) TI 1:1 (2.005 kHz, 2 mA, 0.9 mA/cm^2; and 2 kHz, 2 mA, 0.9 mA/cm^2), and 2) TI 1:3 (2.005 kHz, 1 mA, 0.45 mA/cm^2; and 2 kHz, 3 mA, 1.35 mA/cm^2), as in **Figure 1C** but with two-fold larger amplitudes, and 3) a sham condition (2.005 kHz, 0 mA, 0 mA/cm^2; and 2 kHz, 0 mA, 0 mA/cm^2). We chose a Δf difference frequency of 5 Hz within the theta-band due to the evidential bases for the role of hippocampal theta-band oscillation in episodic memory (Eichenbaum, 2017; Goyal et al., 2020; Staudigl and Hanslmayr, 2013). Stimulation was only applied during the encoding period of each block (i.e., a total 32 s stimulation duration per block, plus 5 s at the beginning and end during which the currents were ramped-up and ramped-down, respectively). Each

participant received only three blocks of each stimulation condition (i.e., a total of 96 s per stimulation condition) in a counterbalanced order between participants.

Participants tolerated well the TI stimulation. There were no adverse effects and only a few incidences of mild common side effects such as concentration difficulty and sleepiness after the experiment that could also be attributed to non-stimulation factors such as the MRI environment (Matsumoto and Ugawa, 2017); see **Table S2** for a detailed summary of the participants' side-effects. Despite the high current densities used, participants did not report significant extraneous sensations, a common concern during conventional transcranial AC stimulation (tACS) (Raco et al., 2014). None of the participants reported perceiving extraneous phosphenes and only a small subset (5 out of 20) reported perceiving a weak extraneous sensation in the skin underneath the electrodes at maximum current intensities. In comparison, when we tested short conventional tACS during setup, all participants reported perceiving extraneous skin sensation underneath the electrodes at a mean current density of 0.225 ± 0.1 SD mA/cm^2 (i.e., at a quarter of the current density used in the experiment with TI stimulation). See **Table S3** for participants' threshold of extraneous sensation.

We first examined whether tuning the current ratio from 1:1 to 1:3 steers the TI stimulation locus towards the Ant hippocampal region, as predicted by our electric modelling (**Figure 1E**). We performed individualised electric field simulations based on participants' anatomical models and electrode locations derived from their structural MRI data (four subjects had to be excluded from the modelling since their electrodes were not visible in the MRI). **Figure 2B** shows the computed amplitudes of the envelope modulation in the Ant, Mid and Post regions of the stimulated hippocampus (relative to total hippocampal exposure as before). We found that TI with 1:1 current ratio resulted in a relatively larger envelope modulation amplitude in the Mid region of the hippocampus (Ant: 0.32±0.03 median±SD, ~13% smaller than Mid; Mid: 0.37±0.02; Post: 0.31±0.03, ~16% smaller than Mid; linear mixed-effects model (LMM) $F_{(2,30)}$= 26.05, p=2.77x10^{-7}; Mid-Post/Ant, p<0.0001, Post-Ant, p=0.42). Changing the current ratio to 1:3 indeed steered the location with the largest amplitude to the Ant region of the hippocampus (Ant: 0.40±0.02; Mid: 0.34±0.01, ~15% smaller than Ant; Post: 0.26±0.02, ~35% smaller than Ant; LMM: $F_{(2,30)}$= 359.62, p< 2.2 x10^{-16}; p<0.0001 across all regions), as was predicted by our simulations in the MIDA model. See **Table S4** for full statistics associated with **Figure 2B**.

We next assessed participants' performance in the task by comparing the objective recall accuracy and recall time, as well as the subjective recall confidence between conditions. Participants selected the target name (i.e. correct face-name association) more frequently than they selected foils or distractors (the probability of a correct selection by chance was 0.2), **Figure 2C**. The recall performance did not differ between stimulation conditions (generalised

linear mixed model (GLMM) /LMM: no main effect of stimulation using multinomial logistic regression $\chi^2(4) = 2.429$, p=0.657 or binomial model (correct vs incorrect responses) $\chi^2(2) = 0.058$, p=0.971), **Figure 2C**. Recall time also did not differ between stimulation conditions, but there was a significant difference in confidence levels explained by a general increase in confidence during the TI 1:3 condition, but no interaction between stimulation condition and response type, **Figure S3** and **Table S5** for full statistics associated with memory performance.

TI Stimulation Reduces Memory Evoked Hippocampal BOLD Signal

After establishing that the TI stimulation can be steered within the regions of the hippocampus without affecting the performance of the associative memory task, we aimed to test whether the stimulation modulated the local neural activity during the task by quantifying change in BOLD signal. The consistency of memory performance across stimulation conditions allowed us to probe the physiological effect of the stimulation on the hippocampal neural activity during memory operation without a confounding contribution from behavioural differences (Driver et al., 2009).

We first examined the BOLD signal during the associative memory task without stimulation (i.e., in the sham condition blocks). **Figure 2D** shows a schematic of the left hippocampus and: i) the relative location of the stimulating electrodes, ii) the anterior-posterior hippocampal axis in an axial orientation. **Figure 2E** shows whole brain change in BOLD signal (relative to the baseline, i.e. rest period) during the encoding and recall periods, illustrating BOLD signal increase in the left hippocampus during encoding but not recall. **Figure 2F** shows the median change in BOLD signal in the left and right hippocampi (extracted from subject-specific hippocampal masks). As expected, we found that BOLD signal increased in both hippocampi during encoding (one-sample t-test, one-sided; left hippocampus $t_{(19)} = 3.698$, p=0.002; right hippocampus $t_{(19)} = 3.921$, p=0.002; FDR corrected), but not during recall stage ($t_{(19)} = -1.281$, p=0.892; right hippocampus $t_{(19)} = -0.250$, p=0.797; FDR corrected), similar to previous reports (Eldridge et al., 2005; Zeineh et al., 2003). The LMM confirmed the significant effect of task stage ($F_{(1,57)}=20.492$, $p=3.09\text{x}10^{-5}$) and lack of hemisphere or interaction between task stage and hemisphere effects (all Fs<0.6, ps>0.4). See **Table S6** for full statistics associated with **Figure 2F**.

The BOLD signal increase in the left hippocampus during encoding was largest in the Ant region (LMM main effect of ROI, $F_{(2,38)}=8.72$, p<0.001; Ant – Mid, p<0.001; Ant – Post, p=0.014; Mid – Post, p=0.55), **Figure 2G** and **Table S7**. Across the left hippocampal regions, the BOLD signal was larger when the memory association was encoded correctly (LMM: main effect of response type (correct vs incorrect), $F_{(1,95)}= 11.09$, p=0.001 and ROI, $F_{(2,95)}= 4.58$, p= 0.012, but no interaction between the two, $F_{(2,95)}= 0.94$, p= 0.39), see **Table S8**. These results

show left hippocampal activity is modulated during formation of correct associations, consistent with previous studies (Sperling et al., 2003). Contrary to the findings in the left hippocampus, the BOLD signal increase in the (not targeted) right hippocampus during encoding was similar across hippocampal regions ($F_{(2,38)}$= 0.20, p= 0.82), and we did not observe a difference in BOLD signal between correct and incorrect encodings (LMM: all Fs<1.4, ps>0.3, see **Table S8**).

We next assessed whether the TI stimulation affected the BOLD signal evoked in the hippocampus by the associative memory task. **Figure 2I** and **Figure 2J** illustrate whole brain BOLD signal during the encoding and recall periods of the TI 1:1 and TI 1:3 stimulation, respectively. **Figure 2K** compares the median BOLD signal in the left, i.e., targeted hippocampus, between stimulation conditions across encode and recall periods. We found that the TI stimulation of the left hippocampus with the 1:1 current ratio did not significantly change the BOLD signal evoked by the associative memory. In contrast, the TI stimulation with the 1:3 current ratio, that steered the stimulation locus to the Ant region, reduced the BOLD signal evoked by the associative memory encoding (LMM: effect of stimulation $F_{(2,95)}$= 3.2, p=0.04; task stage $F_{(1,95)}$= 44.84, p=1.49x10^{-9}; interaction $F_{(2,95)}$= 2.96, p=0.056; Encode: Sham – TI 1:1, p=0.953; Sham – TI 1:3, p=0.006; TI 1:1 – TI 1:3, p=0.015). See **Table S9** for full statistics associated with **Figure 2K**. The stimulation did not significantly affect the BOLD signal in the right hippocampus (LMM: no effect of stimulation or interaction between stimulation and task stage, Fs<2, ps>0.1), see **Table S9** for full statistics associated with **Figure 2L**.

The reduction in the evoked BOLD signal by the TI 1:3 stimulation in the left hippocampus was significant across hippocampal regions, with higher magnitude in the Ant region exposed to the largest relative envelope modulation amplitude (**Figure 2B**), **Figure 2M** (LMM shows effect of stimulation $F_{(2,152)}$= 12.65, p=8.13x10^{-6} and ROI, $F_{(2,152)}$= 6.35, p=0.002; but no interaction between the two p=0.76; Mean Difference: $Ant_{(Sham)}$ - $Ant_{(TI\ 1:3)}$ = 0.18, $Mid_{(Sham)}$ - $Mid_{(TI\ 1:3)}$ = 0.09, $Post_{(Sham)}$ - $Post_{(TI\ 1:3)}$ = 0.14). See **Table S10** for full statistics associated with **Figure 2M**. This pattern was confirmed by inspecting the group-level contrasts comparing stimulation conditions in the left hippocampus. **Figure 2N** shows there were no voxels with significant BOLD differences between sham and TI 1:1 stimulation, whereas during TI 1:3 stimulation there was a reduction in BOLD activity predominantly in the Ant and Post segments of the hippocampus in relation to both sham and TI 1:1 stimulation (percentage of voxels with significant signal change, Sham > TI 1:3: Ant = 30%, Mid = 2%, Post = 25%; TI 1:1 > TI 1:3: Ant = 31%, Mid = 3%, Post = 25%).

In the absence of stimulation, we observed that hippocampal activity was modulated during formation of correct associations, such that BOLD signal was higher for correct than incorrect associations, **Figure 2H**. Similar to the sham condition, the amplitude of the evoked

BOLD signal in the left hippocampus during TI 1:3 stimulation, but not TI 1:1 stimulation, was larger when the memory associations were encoded correctly **Figure 2O** (see **Figure S4** and **Table S11** for full statistics). In addition, the spatial pattern of activity in correct compared to incorrect trials was similar between sham and TI 1:3 conditions, **Figure 2P**. Overall, this indicates that despite a reduction in BOLD signal during the TI 1:3 stimulation, the relative signal difference between correct and incorrect encodings is maintained.

Next, we assessed whether BOLD signal was modulated in the regions underneath and between the stimulation electrodes in the left hemisphere, exposed to a smaller envelope modulation amplitude but a larger absolute field amplitude (**Figure 1H**). There were no significant differences in BOLD signal in these regions, **Figure 2Q** (all ps>0.7, see **Table S12** for full statistics). To support that the lack of changes in BOLD signal was not driven by anatomical variability (as electrode locations were determined using landmarks based on head size) or reduced sample (16 out of 20), we proceeded to extract BOLD signal in the left temporal lobe (excluding the hippocampus) for all participants. There was no significant effect of stimulation on BOLD signal in the left temporal ROI, **Figure 2Ri** (all ps>0.2, see **Table S12**), which was again confirmed by group-level voxelwise analysis, **Figure 2Rii**, showing no significant differences between stimulation conditions. As a final interrogation on the spatial specificity of the BOLD changes, we investigated whether BOLD signal was modulated by stimulation in the left amygdala, located anteriorly to the hippocampus. We did not observe changes in BOLD signal for the left amygdala **Figure S5**. The lack of BOLD signal change in the overlaying cortical regions and neighbouring amygdala cannot be explained by a lack of task activation since, across conditions, we observed evoked BOLD signal in these regions, **Table S13**. Taken together, the distributions of the TI electric fields and induced changes in fMRI BOLD signal demonstrate a non-invasive focal modulation of evoked neural activity in the hippocampus.

The hippocampal decrease in BOLD signal observed during the TI 1:3 condition is in alignment with previous animal studies, showing theta frequency stimulation decreases the magnitude of the BOLD signal in the hippocampus (Angenstein, 2019; Helbing and Angenstein, 2020; Riemann et al., 2017). This would suggest that larger field magnitudes should result in larger decreases in BOLD signal. We observed some evidence to support this relationship (significant Pearson correlations, but no significant robust correlations possibly due to the small sample size) in the same hippocampal regions where BOLD signal was mostly modulated by the stimulation ('Ant' and 'Post' regions), see **Figure S6**.

In this experiment we adopted the premise that the effects of stimulation would be modulated by endogenous activity. Next, we performed an additional experiment in a new cohort of participants where we delivered TI stimulation to the hippocampus in a task that does not elicit hippocampal BOLD activity. In this new experiment, we did not observe modulation

of hippocampal BOLD signal in the absence of endogenous BOLD activity, see **Experiment S1**.

TI Stimulation Modulates Memory Related Hippocampal BOLD Functional Connectivity

Given that successful associative memory involves interactions between the hippocampus and cortical networks, in particular the antero-temporal (AT; more connected to the Ant hippocampal region) and posterior-medial (PM; more connected to the Post hippocampal region) networks (Ranganath and Ritchey, 2012; Ritchey et al., 2015a), we sought to explore whether the stimulation of the hippocampus was associated with changes in the functional connectivity of those networks. **Figure 3A** shows a schematic of the AT/PM networks. We used a generalised psychophysiological interaction (gPPI) method to quantify the effective connectivity for the contrast correct > incorrect, using the Ant, Mid and Post regions of the left hippocampus as seeds and the AT and PM network as targets. The gPPI allowed us to quantify the directional connectivity between the seeds and targets while accounting for task-unrelated connectivity and task-related activity.

We first examined the functional connectivity changes during the associative memory task without stimulation (i.e., in the sham condition blocks). **Figure 3B** shows the functional connectivity between the hippocampal seeds and the AT and PM networks during encode (panel i) and recall (panel ii). We found that the successful encoding of the associative memory increased the functional connectivity between the Ant and Mid, but not Post, hippocampal regions and the AT network. There was no change in the functional connectivity between the hippocampal regions and the PM network (AT: Ant: t=2.322, p=0.022, uncorrected; Mid: t=3.117, p=0.029, FDR-corrected), see **Table S14** for full statistics associated with **Figure 3B**– indicating that the correct associative memory encoding recruited the hippocampal-cortical AT network.

We next explored whether the TI hippocampal stimulation affected functional connectivity during the associative memory task. **Figure 3C** compares the functional connectivity changes during memory encoding between the stimulation conditions. We found that compared to sham, both TI stimulations (TI 1:1 and TI 1:3) reduced functional connectivity between the hippocampus and the AT network. The functional connectivity reduction was localised in the Ant and Mid regions of the hippocampus during TI 1:1 stimulation, **Figure 3Ci**, and in the Mid and Post regions of the hippocampus during TI 1:3 stimulation, **Figure 3Cii** (LMM significant interaction between stimulation type, seed and network $F_{(4,1576)}$= 2.5, p=0.04; post-hoc tests, TI 1:1: Ant, p=0.8; Mid, p< 0.001; Post, p= 0.04; TI 1:3: Ant, p=0.001; Mid, p=0.006; Post, p=0.07). When we compared the functional connectivity between the two TI stimulation conditions, we found a higher relative connectivity at the hippocampal region that

was exposed to the largest envelope modulation amplitude, **Figure 3Ciii**. Specifically, the functional connectivity between the Mid hippocampus and the AT network was larger during TI 1:1 stimulation than during TI 1:3 stimulation (p=0.023). In contrast, the functional connectivity between the Ant hippocampus and the AT network was larger during TI 1:3 stimulation (p=0.008). See **Table S14** for full statistics associated with **Figure 3C** and see **Figure 2B** for the hippocampal envelope modulation distribution. We did not find specific seed-network functional connectivity differences between the stimulation conditions during the recall period; however, we found a main effect of stimulation, explained by lower connectivity values during the TI 1:1 stimulation (LMM main effect of stimulation type: $F_{(2,1576)}$= 8.320, p=2.544x10^{-4}), **Table S15**.

These results suggest that the reduction in the memory evoked BOLD signal in the hippocampus occurred alongside a reduction in the functional connectivity between the hippocampus and its AT cortical network.

Probing the Effect of TI Stimulation on Hippocampal Behavioural Function

To test whether focal hippocampal stimulation could modulate behaviour, we repeated the experimental protocol in a new cohort but with a more extended period of continuous stimulation and a larger number of behaviour trials – an experimental protocol designed to probe behavioural effects of stimulation (Booth et al., 2022). We applied the same electrode configuration as in our earlier studies (**Figure 1B**) to twenty-one healthy human subjects (mean age 23.2 ± 3.7, 10 females) in the TI 1:3 condition (**Figure 1Cii**) that showed stronger modulation of hippocampal memory BOLD signal, and sham. Each participant received only one stimulation condition per session with at least two days between sessions (mean interval 4.9 ± 2.1 days, range 2 – 8 days) in an order counterbalanced between participants. Participants performed the face-name task, as in our original experiment (**Figure 2A**), but with 12 blocks of 16 unique face-name pairs (i.e., a total of 192 association pairs; 4 times more than the original experiment). After encoding, each block included a 40 s distracting task followed by the recall period. Blocks were performed consecutively with a 1-min rest interval after every four blocks. The TI stimulation was delivered continuously throughout each four-block period (i.e., more than 20 times longer continuous stimulation period per condition, delivered not just during encoding but also during the distractor task and recall). In the sham condition, the currents were ramped-up and immediately down at the start and end of each four-block periods. After a period of 30 min, participants were tested again in all face-name pairs. To assess stimulation blindness, we asked participants to report whether they felt that they were stimulated (‘yes’/’no’ response) and their answer’s confidence (scale between 1, not confident, and 10, extremely confident) at four time points during each session, **Figure S7A** shows a schematic of the experimental design.

We first examined stimulation blindness and tolerance. We found that participants were blinded to the stimulation condition. There was no difference between TI stimulation and sham in participants' weighted confidence of receiving stimulation (confidence rates were weighted by +1 for 'yes' and -1 for 'no' answers to the stimulation question as in (Greinacher et al., 2019)), **Figure S7B**. Akin to our earlier studies, participants tolerated the longer TI stimulation periods well, there were no adverse effects and only a few incidences of mild common side effects with only itchiness sensation at the electrode site higher than the sham stimulation (Z = -2.354, p = 0.019), **Table S16** (see **Tables S17** and **S18** for thresholds of extraneous sensations).

TI Hippocampal Stimulation Improves Episodic Memory Performance

We next explored whether the TI stimulation affected the participants' memory performance by comparing the objective recall accuracy and recall time, as well as the subjective recall confidence between conditions, as before. **Figure 4A** shows a summary of the memory performance parameters. In this experiment, employing a longer stimulation duration, we observed an effect of TI stimulation (GLMM: $\chi^2(2) = 6.353$, p = 0.042), **Figure 4Ai**. Participants showed higher proportions of correct (i.e. target) recalls during TI stimulation compared to sham (p = 0.007), with no difference in the number of foils (p = 0.142) or distractors (p = 0.384). We confirmed the higher recall accuracy during TI stimulation employing a frequentist binomial model of correct vs incorrect responses (LMM: $\chi^2(2) = 5.857$, p = 0.016), and Bayesian model, showing posterior distribution estimation of 12% mean accuracy improvement (mean estimate = 0.12, 95% credible interval (CI) = 0.02 to 0.21; 99.15% of the posterior > 0). The total stimulation duration differed slightly between participants due to their self-paced response (total stimulation duration: 34.5 ±3 min, mean ± SD). However, the participants' recall accuracy was not correlated with the stimulation duration (r = -0.045, p=0.85; Pearson correlation).

The participants improvement in the recall accuracy by the TI stimulation was not accompanied with a change in the recall time, **Figure 4Aii** (GLMM/LMM: no main effect of stimulation using multinomial logistic regression $\chi^2(1) = 3.017$, p = 0.082, or binomial model $\chi^2(1) = 2.993$, p = 0.084; and no interaction between stimulation and recall time, ps > 0.2) or confidence rating, **Figure 4Aiii** (LMM: no main effect of stimulation $\chi^2(1) = 0.35$, p = 0.557, or interaction between confidence per response category and stimulation p = 0.809). See **Table S19** for full statistics associated with **Figure 4A**.

We then explored the memory performance during re-test. Not surprisingly, participants performed more poorly during re-test than recall after encoding ($\chi^2(1) = 371.45$, p <0.001, see also **Table S20**)**.** At re-test we did not observe a significant difference between TI

and sham in overall recall accuracy (GLMM: $\chi^2(2) = 3.01$, p = 0.222, **Figure 4Bi**; LMM: $\chi^2(2) = 1.839$, p = 0.175, Bayesian posterior distribution mean estimate = 0.06, 95% CI = -0.03 to 0.16, 90.90% of the posterior > 0), or recall time, **Figure 4Bii** (GLMM $\chi^2(1) = 0.244$, p = 0.622; LMM $\chi^2(1) = 0.255$, p = 0.614). However, because the process of retrieving a memory can transform the information being remembered (Bartlett, 1932; James, 1892), and re-testing can either facilitate or impair the retrieval of information (Finn, 2017), we performed a further analysis to investigate the outcome of each face-name pair from the initial recall to the re-test phase, **Figure 4Biii**. We observed a trend difference between TI and sham (GLMM: $\chi^2(4) = 9.011$, p = 0.061), with further exploratory tests showing that more pairs that were successfully retrieved during TI stimulation were recalled correctly at re-test compared to sham (p = 0.027). This suggests that memories consolidated during TI endure the effects of successive retrievals. See **Table S21** and **Table S22** for full statistics associated with **Figure 4B**.

This experiment required participants to engage in an associative memory task, for which we have shown TI stimulation during the formation of memories modulates BOLD signal in the targeted hippocampus. In an additional behavioural task performed in the same session we applied TI during the execution of a choice-reaction time task. While, in the rodent hippocampus theta oscillations have long been known to be present during voluntary movements, from locomotion to lever pressing (Vanderwolf, 1969; Whishaw and Vanderwolf, 1973), analogous activity in humans related to button presses has been more disputed (Bush et al., 2017; Raghavachari et al., 2001), but see (Halgren, 1991; Mukamel et al., 2010). In our experiment, we observed that for responses provided with the right-hand, contralateral to the left stimulated hippocampus, participants' reaction time was slightly longer and less variable during TI compared to sham, see **Experiment S2**. Our results are in accordance with findings from optogenetic entrainment of theta oscillations in the mouse hippocampus, showing running with less variable and slower speed (Bender et al., 2015).

DISCUSSION

TI is a stimulation strategy whereby neural activity is modulated by applying multiple kHz-range electric fields with a difference frequency within the range of neural activity. We previously validated the concept in rodents and showed the utility of TI stimulation by transcranially stimulating neurons in the hippocampus of living mice without eliciting activity of the overlying cortex (Grossman et al., 2017). We then demonstrated in living rats how focal TI stimulation of the spinal cord could restore functional breathing after an opioid overdose and spinal cord injury (Sunshine et al., 2021). In this paper, we validate the TI stimulation concept in humans. We first use electric field modelling and measurements in a human cadaver to

verify that the locus of the transcranial TI stimulation can be steerably localised to the human hippocampus with minimal exposure of the overlying cortex. We then use neuroimaging and behaviour experiments in healthy human subjects to demonstrate focal noninvasive modulation of the hippocampal memory activity and the capacity to augment memory performance.

Our modelling predicts that the TI fields locus in the hippocampus had a median amplitude of ~0.25 V/m per ~0.45 mA/cm^2 applied current density (1 mA current in our electrodes), consistent with previous TI stimulation computational studies (Huang and Parra, 2019; Lee et al., 2020; Rampersad et al., 2019; von Conta et al., 2021). Yielding a median hippocampal envelope amplitude of ~0.5 V/m in our human studies (~0.9 mA/cm^2 applied current density) and ~0.2 V/m difference between the Ant region and the Mid/Post regions. Similar field amplitudes have been consistently reported to synchronise neural spiking activity tuned to the endogenous oscillation frequency range in-vitro (Reato et al., 2010) and in-vivo (Johnson et al., 2020; Krause et al., 2019; Opitz et al., 2016). One limitation of our cadaver measurements in that data was collected at a temperature that is lower than the living body, resulting in a lower tissue conductivity and, consequently, higher electric field amplitudes for fixed current densities (Opitz et al., 2016). However, since the electric field amplitudes change equally across the head tissues (Opitz et al., 2016), the relative field distribution estimations in the cadaver were not affected.

Our neuroimaging experiments aimed to probe a focal physiological effect. We demonstrate that when the TI stimulation locus is transiently applied to the hippocampus with a theta-band difference frequency during encoding of episodic memory, it reduces the hippocampal evoked BOLD signal without affecting evoked BOLD signal in the overlying cortex. The BOLD reduction was strongest when the TI stimulation locus was steered to the anterior hippocampus, in line with the repeated reports on the central role of this region in the successful encoding of face-name associations (Chua et al., 2007; Sperling et al., 2003; Zeineh et al., 2003). The evidence of focal physiological effect in the hippocampus without behavioural memory differences, enables robust inference of target engagement since memory differences are associated with widespread changes in BOLD signal (Kim, 2011) and can be mediated by remote stimulation of functionally connected sites (Wang et al., 2014) or by stimulation-independent changes in brain state (Otten et al., 2002). In an additional experiment we did not detect a change in hippocampal BOLD signal in the absence of evoked activity, suggesting that TI's ability to modulate BOLD signal is contingent on the level of endogenous activity in the target area.

Our subsequent behavioural experiment aimed to probe the behaviour consequence of the physiological effect in the hippocampus. In this experiment, we substantially extended the period of stimulation, following the evidence that TES modulation of memory performance

in healthy subjects use an average of 17.5 min of continuous stimulation (Booth et al., 2022). We demonstrate that when the TI stimulation is applied to the hippocampus for a more extended period (~20 times longer than before) throughout the episodic memory operation, it provides an improvement in memory accuracy without affecting response time or subjective confidence. We observed that memories formed during TI endured the effects of re-test, but the overall benefit of stimulation was weaker than during initial retrievals. Future studies aimed at understanding long-term effects of stimulation in memory should embed longer intervals between encoding and recall without re-testing, as well as investigate whether more extended stimulation session and/or repeated sessions, may be able to achieve stronger and sustained memory benefits. Those studies may be able to pinpoint the optimal stimulation timing, i.e., memory encoding, maintenance, and/or recall.

What is the possible mechanism by which the theta-band TI stimulation of the hippocampus reduces its memory evoked BOLD response and augments its function? A strong body of evidence shows modulations in theta oscillations in the medial temporal lobe (MTL) during episodic memory (Herweg et al., 2020). Since TI stimulation modulates neural activity at the difference frequency of the kHz-frequency electric fields (Grossman et al., 2017), we anticipate that its application with a theta-band difference frequency will modulate endogenous theta oscillations in the local hippocampal network, resulting in a change in BOLD signal. Whilst the direction of neuronal activity cannot be unambiguously inferred from BOLD responses, and discrepancies in the relationship between BOLD signal and neural activity across cortical and hippocampal regions are well documented (Ekstrom, 2021), our observed reduction of hippocampal BOLD signal due to the TI stimulation is consistent with previous reports in animal models delivering theta frequency electrical stimulation to the hippocampal circuit (Angenstein, 2019; Helbing and Angenstein, 2020; Riemann et al., 2017). Multimodal data, demonstrated that a reduction in hippocampal BOLD signal can be observed alongside increased blood volume and increased spiking activity as a consequence of local increases in deoxyhaemoglobin (Angenstein, 2019; Schridde et al., 2008; Shaw et al., 2021). Although our current data does not allow us to disambiguate which components of the BOLD signal are affected by TI stimulation, it is unlikely that the effect observed can be simply explained by neurovascular changes. This is because no changes in BOLD signal were observed when TI was directed to the Mid hippocampus or in the absence of endogenous BOLD activity (supplementary experiment). Further, changes in functional connectivity were specific to the AT cortical network and their modulation between the two TI conditions was in line with TI fields' distribution along the hippocampal longitudinal axis, providing further evidence of the TI stimulation specificity and steerability. Studies using intracranial electroencephalographic (iEEG) recordings from the hippocampus will be able to elucidate the direct neural response and offer further mechanistic insights to the observed BOLD changes.

Could the change in hippocampal BOLD signal and memory performance have been mediated by stimulation of the overlying cortex exposed to larger field amplitudes? The lack of stimulation effect on the evoked BOLD signal in the overlying cortex and the fact that the participants' change in hippocampal BOLD signal was correlated, albeit weakly, with the envelope modulation amplitude in the hippocampus but not in the overlying cortex render this possibility unlikely.

Could the observed change in hippocampal BOLD signal and memory performance have been mediated by a conventional AC stimulation of the kHz fields in the hippocampus? There is a strong body of evidence showing that the low-pass filtering characteristics of the cell membrane diminish direct membrane depolarization at the kHz range (Bikson et al., 2004; Deans et al., 2007; McIntyre and Grill, 1999; Ranck, 1975). However, there have been reports that invasive stimulation with strong kHz-frequency electric fields can block the propagation of compound action potentials in peripheral nerves (Cuellar et al., 2013; Kilgore and Bhadra, 2014) and improve motor function in patients with Parkinson's disease (Harmsen et al., 2019) potentially via a DC contamination (Franke et al., 2014) or through heating (Khadka et al., 2020). Importantly, these effects were localized to a few millimetres in the vicinity of the implanted electrodes, where the magnitude of the electric fields was exceptionally high. In our study, the cerebral electric fields were generated noninvasively via scalp electrodes with approximately two orders of magnitude lower current densities, resulting in two to three orders of magnitude weaker electric fields in the brain rendering the possibility of such effects very low. Indeed, a recent electrophysiological study investigating the effect of kHz-frequency electric fields in hippocampal brain slices reported no effect on neural activity, even with amplitudes that are two orders of magnitude larger than those we used in this study (Esmaeilpour et al., 2020), consistent with our earlier electrophysiological study in live mouse brain (Grossman et al., 2017).

Across all experiments, the TI stimulation was well tolerated, no adverse effects were recorded, and side effects were mild. We used current densities that are considered safe and in line with those applied across non-invasive electrical stimulation studies, where no serious adverse effects have been reported (Bikson et al., 2016). We found that the thresholds at which TI stimulation produces extraneous sensations, such as tingling undeath the electrodes of phosphenes, are much higher than those for conventional transcranial alternating current stimulation, and allowed for adequate stimulation blinding. This is useful as therapeutical applications might benefit from higher current densities for which blinding becomes harder to achieve (O'Connell et al., 2012).

The hippocampus is important in a myriad of brain functions, including learning and memory, spatial navigation and voluntary movement, and emotional behaviour. It also plays a central role in many of the most common brain disorders, including Alzheimer's disease,

epilepsy, depression and schizophrenia (Small et al., 2011). By modulating the hippocampal neural activity noninvasively, TI stimulation offers new opportunities to probe its causal role in brain functions. In agreement with studies in animal models, we observed that prolonged stimulation of the hippocampus modulated motor behaviour in the contralateral hand. Accumulating evidence suggests that the hippocampus receives bottom-up modulation from subcortical regions and provides top-down feedback to regulate voluntary movements (see (Korotkova et al., 2018) for a recent review), but more substantial research in humans is lacking. Future studies using different electrode configurations and current parameters may sculpt the TI stimulation locus to focally modulate the neural activity in other deep brain structures (see also (Grossman et al., 2018) for translational discussion and contextualization with traditional invasive DBS). Tuning the difference frequency of the applied kHz-frequency fields will allow exploring the frequency band specificity of the target brain regions and contribute to inform stimulation optimisation strategies to treat brain disorders.

MATERIALS AND METHODS

Electric Field Simulations

To characterize the in-vivo exposure to high frequency fields and to low-frequency TI modulation, as well as for the identification of optimized stimulation configurations, dosimetric electromagnetic simulations involving anatomical head models were performed. Two kinds of head models were used: 1) a highly detailed and accurate reference head model, and 2) personalized head models that permit to study the relationship between inter-subject anatomy and exposure variability and subject-specific BOLD response.

Reference Head Model

For maximal simulation realism, the highly detailed MIDA head model (jointly developed with the FDA (Iacono et al., 2015) was used. This model is based on high-resolution (< 0.5 mm throughout) multi-model MRI data, which allows for the distinction of more than 100 different tissue regions, including a range of deep brain targets, the crucial distinction of cancellous and cortical skull layers, the dura, various scalp layers (skin, muscle, fat, tunica) and the complex distribution of cerebrospinal fluid, among other tissues. Co-registered DTI data provides the necessary information about brain heterogeneity and anisotropy, as well as the local principal orientation of fibres.

Personalised Head Models

Individualised (though less accurate and detailed) head models were generated from T1 images (see MRI Data Acquisition) using the SimNIBS framework (version 3.2, (Thielscher et al., 2015)), employing the 'headreco' pipeline (Nielsen et al., 2018) to distinguish six tissue classes: scalp, skull, cerebrospinal fluid, grey matter, white matter, and head cavities. Segmented images were visually inspected and manually corrected when necessary (manual corrections were mostly restricted to the skull-CSF boundary). Because the hippocampi are not included in the automatic segmentation from SimNIBS, these were extracted using FreeSurfer (see Regions of Interest) and converted into tissue surfaces using the iSEG software (IT'IS Foundation, Zurich, Switzerland). Using subject-specific images also permitted to accurately position the scalp electrodes on the reconstructed scalp surfaces in 16 out of 20 participants from experiment 1 (in 4 participants the field-of-view of the T1 image did not allow for a clear localization of the electrodes on the skin).

Electromagnetic field computation

The reference and the reconstructed subject-specific head models were imported as surface mesh entities into the Sim4Life (ZMT ZurichMedTech AG, Zurich, Switzerland) platform with

extended TI modelling functionality. Electrode geometries (2 cm diameter cylinders) were created in Sim4Life, placed at the identified electrode locations, and aligned to the head surfaces, while ensuring gap-less contact. The setup for EM simulations consisted of dielectric property and boundary condition assignment, followed by gridding and voxeling for numerical discretization. The simulations were executed using Sim4Life's finite element method (FEM) low frequency electro-quasistatic, ohmic-current-dominated (EQSCD) solver, that computes solutions to the quasistatic and ohmic-current-dominated approximation of the Maxwell equation ($\nabla\sigma\nabla\varphi = 0$, with boundary conditions) on an adaptive, rectilinear grid, where φ is the electric potential and σ the electric tissue conductivity distribution. EQSCD assumes that ohmic (resistive) currents dominate over displacement currents at the frequencies of interest and that the wave-length is large compared to the computational domain (Bossetti et al., 2008) – conditions that were confirmed by a solver-performed analysis. The conductivities of the non-brain tissues were assigned based on a recent meta-analysis of reported human head electrical conductivity values (McCann et al., 2019). To account for the important impact of brain tissue dielectric anisotropy and heterogeneity, DTI-based electrical conductivity tensor maps were generated. The local main orientation was derived through spectral decomposition of the DTI tensors and in turn combined with the longitudinal and transversal conductivities according to (Hasgall et al., 2018), to reconstruct σ tensors. A convergence analysis was performed to identify an optimal grid resolution that ensures sufficient accuracy (i.e., negligible discretization errors) while minimizing the number of discretization elements (voxels) to reduce computational resource requirements. Simulations were executed at a homogeneous 0.5 mm resolution, which resulted in models consisting of about 80 million voxels. Each TI stimulation exposure condition required the execution of two EM simulations per subject, one for each electrode pair. Dirichlet boundary conditions were assigned to the active electrodes (thus capturing the inhomogeneous current distribution across the electrode interface), applying an arbitrary voltage difference of 1V subject to subsequent current normalization.

Computed TI exposure metrics

The calculated electric (E) fields for each electrode pair were normalized to an input current of 1 mA, by integrating the normal current density over a surface surrounding an electrode. The spatial distribution of the projected TI envelope modulation amplitude along the local brain structure orientation $\vec{n}$ was computed from the fields of both electrode pairs using $\left|\vec{E}_{AM}(\vec{n},\vec{r})\right| = \left|\left|\left(\vec{E}_1(\vec{r}) + \vec{E}_2(\vec{r})\right)\cdot\vec{n}\right| - \left|\left(\vec{E}_1(\vec{r}) - \vec{E}_2(\vec{r})\right)\cdot\vec{n}\right|\right|$ where $\vec{E}_1(\vec{r})$ and $\vec{E}_2(\vec{r})$ are the fields generated by the first and second electrode pair, respectively, at the location $\vec{r}(x,y,z)$. The local brain structure (e.g., white-matter fibres, organized pyramidal neurons in the hippocampus) orientation was identified as the principal axis of the corresponding DTI tensor.

Electric Field Measurements in Human Cadaver

A human male cadaver (93 years old) with no known brain disorder was provided by the "service des corps donnés à la science" by Aix Marseille Université. Experiments were performed in the Faculty of Medicine La Timone (Aix Marseille Université). The subject was perfused with zinc chloride, stored in freezer until the experiments and left to warm to 20°c before the recording session.

Electric fields were recorded using three stereoelectroencephalography (sEEG) 15-contact electrodes, ring diameter 0.8 mm, length 2 mm, useful exploration length 51 mm (Alcis, Besançon, France, 2069-EPC-15C-35). The sEEG electrodes were implanted in the left mesial temporal lobe, perpendicular to the hippocampal longitudinal axis. The technique of implantation was based on the neurosurgeon's experience in performing SEEG (RC) and was similar to the one routinely applied to human patients for the presurgical work-up of drug-resistant epilepsy. Each electrode was orthogonally inserted through a short 20-mm guidance screw (Alcis, Besançon, France, 2023-TO-C-020) after 2.5 mm diameter drilling of the bone. Reference and ground electrodes were placed on the shoulder of the cadaver using ECG electrodes (WhiteSensor WS, Ambu® Inc., MD, USA, 1.5x1.5 cm).

The electric potential signals from the sEEG electrodes were amplified and sampled at 30 kS/s using the RHS Stim/Recording Controller (Intan Technologies, Los Angeles, CA, USA). The stimulating currents were applied using 1.5 cm x 1.5 cm scalp electrodes (WhiteSensor WS, Ambu® Inc., MD, USA) configured as in **Figure 1B**. The two currents were generated using two electrically isolated current sources (DS5, Digitimer Ltd., UK) driven by voltage waveforms from a function generator (Keysight, EDU33212A, Santa Rosa, California, USA). In the case of TI stimulation, we applied one current at 2.005 kHz frequency and 1 mA (current density ~0.45 mA/cm^2) amplitude and a second current at 2 kHz frequency and same amplitude (i.e., TI with Δf = 5 Hz and 1:1 current ratio, **Figure 1Ci**). In the case of conventional tACS, we applied two currents at 5 Hz frequency and 1 mA amplitude. Each stimulation condition was applied for 25 s. The 3D location of the electrodes within the expected mesial temporal anatomical targets was confirmed by a CT of the head at the end of the experiment, see **Figure 1F**.

The recorded data were analysed using a custom-written script in MATLAB (Mathworks, Natick, MA). The electric potential signals were first bandpass filtered using a 1st order Butterworth filter with cut-off frequencies of 0.5 kHz and 5 kHz in the case of TI stimulation and 1 Hz and 40 Hz in the case of conventional tACS. The normalised envelope modulation amplitude in each electrode was estimated by first extracting the recorded signal's envelope waveform using a Hilbert transform and a low-pass filter (i.e., 1st order Butterworth

filter with a cut-off frequency of 0.5 kHz) and then computing the mean half difference between the waveform maxima and minima (averaged first in 1 s epochs and then across the 25 epochs). The envelope modulation amplitude of each electrode was then normalized to the largest envelope modulation amplitude across the electrode's contact points. The envelope modulation ratio was estimated by dividing the amplitude of the envelope waveform by the maximum signal amplitude. The field's envelope modulation amplitude along the axis of the recording electrodes (i.e., perpendicular to the hippocampal longitudinal axis) was estimated by computing the difference in envelope modulation amplitudes between neighbouring contact points and dividing the value by the inter contact distance. The normalised absolute amplitude in each electrode was estimated by computing the median value of the signal maxima (again averaged first in 1 s epochs and then across the 25 epochs). The field's amplitude along the axis of the recording electrodes (i.e., perpendicular to the hippocampal longitudinal axis) was estimated by computing the difference in amplitudes between neighbouring contact points and dividing the value by the inter contact distance. The spatial maps of the normalised envelope modulation amplitude and normalised absolute amplitude were created by first applying a 3-point moving average over the electrode contacts followed by a linear interpolating of the electrode contact values of 100 x 151 grid.

Hilbert transform was applied to TI data, followed by low-pass filtering (500 Hz) using a first order zero-phase, forward-reverse Butterworth filter. Maximum and minimum amplitudes were computed by calculating the median values extracted from 1 s epochs. The amplitude envelope modulation for TI data was calculated using the average of the maximum and minimum amplitudes. The envelope modulation ratio was calculated as the ratio of the envelope modulation amplitude to the maximum amplitude. Field strengths were calculated using the first spatial derivative of the envelope modulation amplitude or maximum amplitude.

Human Subjects – in-vivo experiments

Twenty-two healthy volunteers were recruited for the MRI experiment (Face-name memory task during fMRI acquisition) and twenty-one for the experiment probing the effects of TI stimulation on behaviour. See Supplementary Materials and Methods for Experiment S1.
In the fMRI experiment, two participants were excluded, one because of technical difficulties with the MRI scanner (no images were collected) and another due to excessive movement in the scanner. Thus, the final cohort for this experiment was composed of twenty subjects (11 females, age range: 20 to 54 years old, mean age 27.1 ± 7.6 SD, 19 right-handed and 1 left-handed). For the behavioural experiment, all participants were included in the analysis (10 females, age range: 19 to 32 years old, mean age 23.2 ± 3.7 SD, all right-handed). All subjects were educated to degree level or above with no self-reported history of neurological or

psychiatric illness. Participants gave written informed consent. The study conforms to the Declaration of Helsinki and ethical approval was granted by the Imperial College Research Ethics Committee (ICREC). MRI data was collected at Imperial College London clinical imaging facility (CIF).

Face-Name Task

The task was designed using the Psychtoolbox (Brainard, 1997) for Matlab (Mathworks, Natick, MA). In the MRI experiments, responses were collected with a response box (NordicNeuroLab, Norway) that was connected to the stimulus presentation PC through a fibreoptic. In the behavioural experiment, responses were collected using a computer keyboard connected to the stimulus presentation PC. The order of the stimulation was counterbalanced across participants using a balanced Latin square. This allowed us to keep factors of no interest fixed (i.e., difficulty of a specific block or tiredness), while controlling for the variable of interest, i.e. stimulation condition.

The Face-Name task was chosen based on a strong body of evidence demonstrating that face-name associations are dependent on hippocampal function and elicit bilateral hippocampal activations in healthy subjects (Chua et al., 2007; Sperling et al., 2003; Zeineh et al., 2003). Faces were retrieved from the Chicago Face Database v.2.0.3 (Ma et al., 2015) and names from the Office for National Statistics (Baby Names, England and Wales, 1996; which corresponds to the dataset closest to the mean age for the faces in the Chicago Face Database, mean age = 28 years old). We selected names that had between 5 and 7 letters. Names present in both female and male lists were removed (e.g. Charlie) and if the same name was present with a different spelling (e.g. Elliot and Elliott) only the one with the highest frequency was kept. The task was composed of 9 blocks in the fMRI experiment and 12 blocks in the behavioural experiment, each containing 16 unique face-name pairs of different ethnicities (4 black female, 4 black male, 4 white female and 4 white male per block; all with neutral facial expressions). The task was composed of an encoding and a recall stage. During the encoding stage each face-name pair was displayed for 2 s. Faces were displayed in the centre of the screen with the name underneath (**Figure 2A**). Participants were instructed to read the name underneath the faces and try to learn each face-name pair. This was followed by either a delay period (16 s) where a fixation cross was present in the centre of the screen in experiment 1, or a distractor task (40 s) where participants made odd/even judgments for random integers ranging from 1 to 99 (to prevent maintenance of information in working memory) in the behavioural experiment. In the recall stage, participants were shown each face with 5 names underneath: the target name, two distractor names (i.e., names that were not present in the block), and two foil names (i.e., names that were present in the block but associated with a different face) - target and distractor names were selected to have a similar

name frequency. Each name appeared in black font, inside a grey rectangle and the temporally selected rectangle was coloured in cyan. Participants moved between rectangles (using left and right index buttons in the fMRI experiment or left and right arrow keys in the behavioural experiment) and pressed a key to confirm their selection (right thumb in the fMRI or space bar in the behavioural experiment). This was followed by a confidence rating, in which participants were asked to rate how confident they were in their selection from 1 to 4 (1 being not confident at all and 4 extremely confident). Selection was made using the same procedure described for the name selection. For the recall stage, participants were instructed to respond as quickly and as accurately as possible. There was a time limit (20 s in the fMRI experiment and 8 s in the behavioural experiment) to select each name and to rate the confidence level (5 s in experiment 1 and 3 s in experiment 3). The order of the blocks was kept constant across participants, but the order of the face-name pairs was pseudo-randomised across participants, such that no more than three faces of the same type appeared in a row. The order of face recall was randomised across participants, and the last two encoding trials were never presented at the beginning of the recall. The position of the names in the recall stage was also randomised. In the behavioural experiment, participants performed a re-test, 30 minutes after the last recall block. During this period participants were asked to recall the names matching all faces presented for that session. Stimuli were grouped in their original blocks, but blocks presented in a different order from the recall after encoding and the order of the stimuli randomised per block. The order of the blocks in the re-test was kept constant between sessions, with unique stimuli presented in each session. Confidence ratings were not collected during re-test. Participants watched a nature video between the last block of the recall period and the re-test. There was one video per session and all participants watched the same video.

Behavioural Analyses

Three main variables of interest were analysed, i.e., response type, reaction time for name selection and confidence level (reaction times for confidence were also recorded but not analysed). For each face-name trial four response types were possible at the recall stage: 1) correct association, selection of the correct name for the face presented; 2) foil (incorrect association), selection of a name that was present in the same block but did not match the face (2 foils were present per recall trial); 3) distractor (incorrect association), selection of a name that was not associated to any face across all blocks (2 distractors were present per recall trial); 4) omission, participant did not select a response within the time limit.

We first assessed accuracy across the whole task (correct vs incorrect associations) to check whether any participant had an overall performance below chance (20%), which would exclude them from further analyses. All participants were above chance (fMRI

experiment: mean = 49.97%, SD = 9.77%, range 32.64 – 70.83 %; behavioural experiment – recall: mean = 58.47%, SD = 14.73%, range 33.85 – 91.15%). The distribution of responses for correct associations, foils and distractors across the whole task followed the expected pattern, with higher percentage of responses for correct associations than foils than distractors, indicating appropriate engagement with the task (fMRI experiment: correct associations = 50%, foil = 33.3%, distractor = 16.5%, omission = 0.17%; behavioural experiment – recall: correct associations = 58.46%, foil = 24.76%, distractor = 12.29%, omission = 4.49%). The number of omissions was considered negligent and removed from the dataset. We then plotted reaction times across the whole task; this showed a right-skewed distribution, typical for this metric. To trim the distribution, we calculated the 1 and 99 percentiles across all trials and participants and dropped trials below or above these thresholds.

To investigate whether the number of responses differed per response type across stimulation conditions we performed a multinominal logistic regression on the trial-by-trial data using the multinom function in the *net* package in R (Venables and Ripley, 2002). The outcome variable response type contained three levels, correct, foil, distractor, and the level "correct" was used as the intercept, with predictors for stimulation type (sham, TI 1:1, TI 1:3 in the fMRI experiment and sham and TI 1:3 in the behavioural experiment), *p* values were calculated using Wald tests. In addition, as we were interested in investigating the contrasts for correct and incorrect responses in the imaging data, we defined a binomial generalised linear mixed model (GLMM) using a logistic link function to model the effect of stimulation type on accuracy (correct vs incorrect associations). The final model included random intercepts for participant and task block (task block was not a variable of interest, as blocks were counterbalanced across stimulation conditions and was included for appropriately modelling variance in the data). In the behavioural experiment, we included in addition random intercepts for session, and modelled accuracy used Bayesian mixed effect models using the *brms* package (Bürkner, 2017). Bayesian frameworks are robust to potential violations of normality or homoscedasticity and allow considering whether an effect is credibly different from a null value. The Bayesian model included random intercepts for participants, session, and blocks.

To investigate whether reaction times differed per response type across stimulation conditions the data was modelled with GLMM using an inverse Gaussian distribution with the identity link function (Lo and Andrews, 2015). The final model included random intercepts for participants and blocks in the fMRI experiment and for participants, session and trial nested in blocks in the behavioural experiment. We also run an additional model using accuracy instead of response type, to investigate whether reaction times differed by accuracy and stimulation type (again employing the inverse Gaussian distribution with the identity link function and random intercepts as described above).

Finally, we investigated the participants confidence levels for the selected face-name associations. First, we removed trials where participants did not specify a confidence level within the time limit (fMRI experiment: 0.28% trials; behavioural experiment: 0.78% trials). To investigate whether confidence levels (ordinal variable) differed per response type across stimulation conditions, the data was modelled using a cumulative link mixed model (logit link function) using the "clmm" function from the *ordinal* package in R (Christensen, 2019).

Statistical procedures

All statistical analyses were conducted using R version 3.6.0 via RStudio and plots were generated with the ggplot2 package. GLMM models used the glmer function and LMM models the lmer function, from the *lme4* package with *p* value approximation performed by the *lmerTest* package in R (Bates et al., 2015; Kuznetsova et al., 2017). Bayesian models were implemented using the *brms* package (Bürkner, 2017). We ran a minimum of 2000 iterations over four MCMC chains, with a 'warm-up' period of 1000 iterations per chain leading to 4000 usable posterior samples, visual inspection of all MCMC results revealed satisfactory Rhat values (<1.01). In these analyses, an effect is seen as statistically significant if the credible interval does not contain zero with 95% certainty.

Temporal Interference (TI) stimulation

TI stimulation was delivered using a custom-made device as described in (Grossman et al., 2017). Two sinusoidal waveforms (at frequencies 2 kHz and 2.005 kHz) were supplied via a balanced pair of current sources that were driven in precisely opposite phase with a ground electrode carrying any imbalance currents (< 1%) from the paired current sources, preventing charging of the body relative to earth ground. Two pairs of stimulation electrodes (self-adhesive TENS, 1.5 cm x 1.5 cm with the corners cut to produce a rounded shape), were positioned on the participants' heads using a conductive paste (Ten20, D.O. Weaver, Aurora, CO, USA) and held in place using medical tape (3M™ Micropore ™ medical tape). Electrode 1 (*e*1) and electrode 3 (*e*3) were positioned on the left hemisphere at the level of the nasion plane, *e*1 was positioned anterior to *e*3 (*e*1 at 50% of the subject's half circumference minus 2.5 cm and *e*3 at 50% of the subject's half circumference plus 2.5 cm, both counting from the nasion; such that the centres of the electrodes were 5 cm apart). Electrodes 2 and 4 (*e*2 and *e*4) were positioned on the right hemisphere at a plane just above the eyebrow, *e*2 was positioned anterior to *e*4 (*e*2 at 20% of the subject's half circumference minus 1 cm and *e*4 at 70% of the subject's half circumference plus 1 cm, both counting from the nasion). *e*1-*e*2 formed one electrode pair and *e*3-*e*4 the second electrode pair, **Figure 1B**.

Stimulation was applied in two conditions: 1) TI stimulation directed to the mid left hippocampus: a current of 2 mA was applied to both electrode pairs, i.e., a current ratio 1:1 ('TI 1:1' condition); 2) TI stimulation steered to the anterior left hippocampus: a current of 1 mA was applied to the electrode pair *e1*-*e2* and a current of 3 mA was applied to the electrode pair *e3*-*e4*, i.e., a current ratio 1:3 ('TI 1:3' condition). In both conditions, the stimulation began with a 5 s ramp-up and ended with a 5 s ramp-down. Sham stimulation was equivalent to the TI 1:1 stimulation condition in the fMRI experiments, but the current was ramped down to zero immediately after it was ramped-up. In the behavioural experiment, sham stimulation was equivalent to the TI 1:3 condition, with an initial period of 30 s of stimulation followed by ramp-up and ramp-down periods at the beginning and end of the CRT task and at the beginning and end of four consecutive blocks of the face-name task, see **Figure S7A**. The duration of stimulation was kept constant across participants for the fMRI experiment(96 s per stimulation condition), but durations varied between participants for the behavioural experiment where TI was applied throughout the face-name task blocks and responses were self-paced (stimulation during face-name task: mean ± SD, 34.5±3 min, range 29.37±40.35 min; total stimulation duration TI session: 44.53±3 min, range 39.37 – 50.35 min, which includes 10 min of stimulation before the face-name task, see **Figure S7A**).

The beginning and end of each stimulation block/period was controlled via an external trigger, sent from the computer running the experimental paradigm to the stimulator (triggers were sent from MATLAB using serial port commands). In the fMRI experiments, the start of each block was triggered by a signal from the MR scanner, this ensured that task and stimulation were synchronous to the scanner clock. The stimulator was placed outside the MR shielded room and the currents from the stimulator were delivered into the scanner room via RF filters, one placed in the operator room and another inside the scanner bore (NeuroConn GmbH, Ilmenau, Germany). The filter inside the MRI bore was connected to the stimulation electrodes via two MR compatible stimulation cables (NeuroConn GmbH, Ilmenau, Germany). Phantom and pilot experiments were initially conducted to ensure that the experimental setup did not introduce artifacts in the fMRI signal. Additionally, we estimated total signal-to-noise ratio (tSNR) in the fMRI signal in the brain regions underneath the electrodes on the left hemisphere and their contralateral equivalents (i.e., regions of interest, ROIs) to assess whether the presence of the electrodes had an effect on the quality of the signal. tSNR was calculated by dividing the mean of the signal over time by the standard deviation over the whole fMRI acquisition, **Figure S8**.

Brain Stimulation Procedure

Before each experiment, the participants' sensation and comfort were tested. The participants were first exposed to low frequency stimulation followed by TI stimulation, for each electrode

pair at a time, first *e*1- *e*2 followed by *e*3- *e*4. Stimulation started at 0.1 mA and increased in steps of 0.1 mA until participants reported any sensations associated to stimulation (i.e., pins and needles, burning, phosphenes, etc.) or until maximum intensities for the experimental protocol were reached (2 mA for *e*1- *e*2 and 3 mA for *e*3- *e*4). A detailed description of perceptual sensations and thresholds is provided in **Table S3**, **Table S17** and **Table S18**. At the end of the experiments, participants completed a questionnaire to assess possible side-effects of TI stimulation by rating from 0 (none) to 4 (severe) the intensity and duration of: pain, burning, warmth/heat, itchiness, pitching, metallic taste, fatigue, effect on performance, trouble concentrating, sleepiness/fatigue, headache, mood change, or any other side-effect perceived. A detailed description of side effects, their intensity and the number of incidences is reported in **Table S2** and **Table S16**. In the behavioural experiment we compared the strength ratings of the side effects using Wilcoxon signed-rank tests performed using the *coin* package (Hothorn et al., 2008).

Effectiveness of sham blinding

In the behavioural experiment, where we had separate active and sham sessions, we included an additional protocol to investigate the effectiveness of sham blinding by asking at 4 timepoints during each session the following questions: “Do you think you had stimulation” (yes/no) and “How confident are you?” (1 is not confident at all – 10 is extremely confident). Participants responded to each question by using an editable form in pdf format. Following (Greinacher et al., 2019), we combined the two questions into a weighted score, whereby a “yes” answer was assigned a +1 value and “no” answer a value of -1, which were then multiplied by the confidence rating. We extracted the median and 95% confidence intervals for each time point and each stimulation condition using a smooth bootstrap technique (Brown et al., 2001) implemented in the *kernelboot* package (Wolodzko, 2020). We used a Gaussian kernel and 10000 permutations for each probe point.

MRI Data Acquisition

Scanning was performed in a 3T Siemens Verio (Siemens, Erlangen, Germany) at the Imperial College’s CIF, using a 32-channel head coil. Standard T1-weighted structural images were acquired using a magnetization-prepared rapid gradient-echo (MP-RAGE) sequence, 1 mm^3 isotropic voxel, repetition time (TR) 2.3 s, echo time (TE) 2.98 ms, inversion time 900 ms, flip angle (FA) 9°, field of view 256 × 256 mm, 256 × 256 matrix, 160 slices, GRAPPA acceleration factor = 2. Field map scans were acquired to correct the echoplanar imaging (EPI) images for signal distortion (TR = 599 ms, TE = 7.65 ms, FA = 60°). FMRI images were obtained using a T2*-weighted gradient-echo EPI sequence, 3 mm^3 isotropic voxel, TR 2 s, TE 30 ms, FA = 80°, field of view 192 × 192 × 105 mm, 35 slices, GRAPPA acceleration factor = 2. A total of

804 volumes were acquired on average (range: 592 – 1162), times varied depending on how long participants took on the recall stage of the task.

Regions of Interest

Regions of interest (ROIs) included: 1) the hippocampi, 2) their longitudinal parcellations; 3) regions corresponding to the AT-PM networks, and 4) regions corresponding to the cortical regions overlying the stimulated hippocampus, i.e., underneath and between the stimulating electrodes *e1* and *e3*.

Hippocampal masks were defined based on the segmentation of the whole hippocampi performed for each subject using the pipeline for automated hippocampal subfield segmentation in FreeSurfer (version 6.0.0, (Fischl, 2012; Iglesias et al., 2015)). The hippocampal masks were normalised to MNI and split into thirds along the long axis of the hippocampus ((Collin et al., 2015); posterior portion of the hippocampus: from Y = −40 to −30; mid-portion of the hippocampus: from Y = −29 to −19; anterior portion of the hippocampus: from Y = −18 to −4, **Figure 1Ei**). The inverse normalization parameters were used to create subject specific parcellated ROIs and used in the subject space for fMRI analyses.

ROIs for the AT-PM networks were defined following (Cooper and Ritchey, 2019) using regions previously identified as belonging to distinct networks through resting state and functional connectivity analyses during associative memory encoding (Libby et al., 2012; Ritchey et al., 2014). AT regions included the bilateral perirhinal cortex, amygdala, anterior fusiform gyrus, anterior inferior temporal cortex, and lateral orbitofrontal cortex. PM regions included the parahippocampal cortex, posterior cingulate cortex, precuneus and angular gyrus. The ROIs were obtained from probabilistic atlases thresholded at 50%, including a medial temporal lobe atlas (https://neurovault.org/collections/3731/; (Ritchey et al., 2015b)) for parahippocampal cortex and precuneus, and the Harvard-Oxford cortical and subcortical atlases for all other regions (**Figure 3A**).

ROIs for the cortex overlying the stimulated hippocampus were defined for each subject. Using the anatomical T1 images, one ROI was placed underneath the anterior stimulating electrode *e1* (i.e., ROI Crtx Ant) and a second ROI was placed underneath the posterior stimulating electrode *e3* (i.e., ROI Crtx Post). The third ROI was placed in the middle between the electrodes (i.e., ROI Crtx Mid). All cortex ROIs were 10 mm spherical masks. See **Figure 1Di.** The positions of the electrodes on the left hemisphere were visible in 16 out of the 20 participants (see Personalised EM Models section).

We extracted two additional sets of ROIs for control measurements: the left amygdala (using a procedure analogous to the individual hippocampal ROIs) and cortical ROIs in the

right hemisphere (same axial plane as the left hemisphere ROIs). All ROIs were converted to the subject space for fMRI analyses.

FMRI Data Pre-processing

Data were pre-processed using FMRIB Software Library (FSL version 6.0.1, (Jenkinson et al., 2012; Smith, 2004). Functional data were pre-processed using the FMRI Expert Analysis Tool (FEAT), including motion correction using MCFLIRT (Jenkinson et al., 2002), distortion correction using fieldmap images prepared from fsl_prepare_fieldmap, slice-time correction using Slicetimer, smoothing with a 3D Gaussian kernel (8 mm full-width at half maximum, FWHM) and high-pass filtered at a cut-off of 0.008 Hz. Skull stripping was performed using FSL's BET (Smith, 2002). Head motion was estimated using FSL motion outliers through DVARS (the spatial root mean square of the data after temporal differencing) (Power et al., 2012). Criterion for excessive motion was DVARS > 0.5 in more than 20% of the volumes. In experiment 1 (i.e., Face-name task), one subject was excluded based on this. For the sample included in the analyses for the fMRI experiment, mean DVARS and SD were 0.25 and 0.03 respectively. There was no difference in motion across stimulation conditions ($F_{(2,38)}$=1.03, p=0.367).

FMRI Analysis

For each participant, pre-processed fMRI data was modelled using three different GLMs, two designed for univariate analyses and a third for assessing functional connectivity using generalised psychophysiological interaction (gPPI), (McLaren et al., 2012). In addition to the explanatory variables (EVs) of interest (described below), all GLMs included as nuisance regressors twenty-four motion parameters (six motion parameters - translation and rotation in three directions, the square of the six motion parameters and their temporal derivatives) and a regressor with volume outliers identified by DVARS to model out volumes (i.e., scrubbing) with extensive motion.

The first GLM was used to analyse univariate BOLD effects during encode and recall periods of the task and included 3 EVS for encode and 3 EVS for recall (one EV per stimulation condition and task stage) and their first temporal derivatives. Regressors were created by convolving a boxcar kernel with a canonical double-gamma hemodynamic response function.

The second GLM analysed univariate BOLD effects for correct and incorrect trials during encode and recall periods. This was possible without temporal jittering because we obtained a balanced distribution between correct and incorrect responses and the ordering of trials was randomised as a consequence of subject performance and pseudo-randomization of the stimuli presentation across participants (Burock et al., 1998). This model included 12

EVs (one for correct and another for incorrect trials for encode and recall periods per stimulation condition), 3 EVs for the confidence intervals (one per stimulation condition) and their first temporal derivatives. Regressors were created by convolving a boxcar kernel with a canonical double-gamma hemodynamic response function.

The third set of GLMs, used to assess functional connectivity with gPPI, included 25 EVs, describing physiological, psychological and PPI regressors. Physiological regressors were defined from the fMRI time-course extracted from seeds in the Ant, Mid and Post left hippocampus (see ROI definition). The psychological regressors included those modelled for the second GLM. For each model (one per seed), the physiological term and the psychological term were used to create the PPI interaction terms.

Using the output of the first GLM we assessed the fMRI BOLD signal to the encode and recall periods of the task (contrasted against the baseline), first for the sham condition and then for each stimulation condition (**Figure 2**). Using the output of the second GLM, we measured BOLD response to correct and incorrect associations during the encode period of the task (contrasted against the baseline), first for the sham condition and then for all stimulation conditions (EVs 1-12). The contrast correct > incorrect was also used to extract connectivity values in the gPPI models described above.

FMRI Statistics

Whole brain BOLD activity at the group level was visualised by employing mixed effects analyses using FLAME 1 (Beckmann et al., 2003; Woolrich et al., 2004). Z statistical images were thresholded using Gaussian Random Fields based cluster inference with an initial cluster-forming threshold of $Z>3.1$ and a family-wise error (FWE) corrected cluster-extent threshold of $p<0.05$.

Statistical analyses of fMRI data were performed using the model estimates (in percent BOLD signal change) from the ROIs defined *a priori*. For each subject, we employed FSL Featquery tool to interrogate timeseries associated statistics, for each of the contrasts defined above, in the regions of interest in the subject space (see ROI specification). For analysis of the BOLD magnitude, we used the median % BOLD signal change (as the mean values were often not normally distributed) and for connectivity analysis we used the means.

ROI statistical analyses were conducted using R version 3.6.0 and plots were generated with the ggplot2 package. All mixed-effect models were fitted using the function lmer from the *lme4* package in R. ANOVA Type II Wald F tests with Kenward-Roger approximation for degrees of freedom or Type II Wald Chi-square tests were performed using the function Anova() for *p*-value approximation. Post hoc Tukey's comparisons were made using the estimated marginal means from the *emmeans* package. The level of statistical significance was set at $p<0.05$ for all tests.

Voxelwise analyses within ROIs was performed using FSL's randomise tool with 5,000 permutations and family-wise error correction for multiple comparisons using threshold-free cluster enhancement (TFCE). All statistical maps were family-wise corrected and thresholded at $p < 0.05$.

Code and Data Availability

The code for the face-name task is available on Gitlab (https://gitlab.eps.surrey.ac.uk/nemo/facenametask). Data and key scripts are available on Gitlab (https://gitlab.eps.surrey.ac.uk/nemo/ti-paper). Group-level data used to generate the fMRI figures are available in NeuroVault (https://neurovault.org/collections/11908/).

ACKNOWLEDGEMENTS

I.R.V. is supported by the Biotechnology and Biological Sciences Research Council (BB/S008314/1). A.H. is supported by the UK Dementia Research Institute Care Research and Technology Centre and Biomedical Research Centre at Imperial College London. E.S.B was supported by Lisa Yang, John Doerr, HHMI, NIH R01MH117063, and Edward and Kay Poitras. N.G. was funded by the UK Dementia Research Institute (UK DRI)—an initiative funded by the Medical Research Council, Alzheimer's Society and Alzheimer's Research UK, Wellcome Trust fellowship (097443/Z/11/Z), Science & PINS Award for Neuromodulation, and NIHR IBRC Confident in Concept Award. A.W. is supported by the European Research Council (ERC) under the European Union's Horizon 2020 research and innovation programme (716867). D.K is supported by the University of Surrey's Vice-Chancellor Scholarship Award.

DECLARATION OF INTERESTS

N.G. and E.S.B are inventors of a patent on the technology, assigned to MIT.

E.S.B., N.G., N.K., A.P-L. and E.N. are co-founders of TI Solutions AG, a company committed to producing hardware and software solutions to support TI research.

REFERENCES

Angenstein, F. (2014). The actual intrinsic excitability of granular cells determines the ruling neurovascular coupling mechanism in the rat dentate gyrus. J Neurosci *34*, 8529-8545.

Angenstein, F. (2019). The role of ongoing neuronal activity for baseline and stimulus-induced BOLD signals in the rat hippocampus. Neuroimage *202*, 116082.

Antal, A., and Paulus, W. (2013). Transcranial alternating current stimulation (tACS). Front Hum Neurosci *7*, 317.

Bartlett, F.C. (1932). Remembering: A study in experimental and social psychology (Cambridge: Cambridge University Press).

Bates, D., Mächler, M., Bolker, B., and Walker, S. (2015). Fitting Linear Mixed-Effects Models Using lme4. 2015 *67*, 48.

Beckmann, C.F., Jenkinson, M., and Smith, S.M. (2003). General multilevel linear modeling for group analysis in FMRI. Neuroimage *20*, 1052-1063.

Benabid, A.L., Chabardes, S., Mitrofanis, J., and Pollak, P. (2009). Deep brain stimulation of the subthalamic nucleus for the treatment of Parkinson's disease. Lancet Neurol *8*, 67-81.

Bender, F., Gorbati, M., Cadavieco, M.C., Denisova, N., Gao, X., Holman, C., Korotkova, T., and Ponomarenko, A. (2015). Theta oscillations regulate the speed of locomotion via a hippocampus to lateral septum pathway. Nat Commun *6*, 8521.

Bikson, M., Grossman, P., Thomas, C., Zannou, A.L., Jiang, J., Adnan, T., Mourdoukoutas, A.P., Kronberg, G., Truong, D., Boggio, P.*, et al.* (2016). Safety of Transcranial Direct Current Stimulation: Evidence Based Update 2016. Brain Stimul *9*, 641-661.

Bikson, M., Inoue, M., Akiyama, H., Deans, J.K., Fox, J.E., Miyakawa, H., and Jefferys, J.G. (2004). Effects of uniform extracellular DC electric fields on excitability in rat hippocampal slices in vitro. J Physiol *557*, 175-190.

Booth, S.J., Taylor, J.R., Brown, L.J.E., and Pobric, G. (2022). The effects of transcranial alternating current stimulation on memory performance in healthy adults: A systematic review. Cortex *147*, 112-139.

Bossetti, C.A., Birdno, M.J., and Grill, W.M. (2008). Analysis of the quasi-static approximation for calculating potentials generated by neural stimulation. J Neural Eng *5*, 44-53.

Brainard, D.H. (1997). The Psychophysics Toolbox. Spat Vis *10*, 433-436.

Brown, B.M., Hall, P., and Young, G.A. (2001). The smoothed median and the bootstrap. Biometrika *88*, 519-534.

Bürkner, P.-C. (2017). brms: An R Package for Bayesian Multilevel Models Using Stan. Journal of Statistical Software *80*, 1 - 28.

Burock, M.A., Buckner, R.L., Woldorff, M.G., Rosen, B.R., and Dale, A.M. (1998). Randomized event-related experimental designs allow for extremely rapid presentation rates using functional MRI. Neuroreport *9*, 3735-3739.

Bush, D., Bisby, J.A., Bird, C.M., Gollwitzer, S., Rodionov, R., Diehl, B., McEvoy, A.W., Walker, M.C., and Burgess, N. (2017). Human hippocampal theta power indicates movement onset and distance travelled. Proc Natl Acad Sci U S A *114*, 12297-12302.

Christensen, R.H.B. (2019). ordinal—Regression Models for Ordinal Data. In R package version 2019 12-10 https://CRANR-projectorg/package=ordinal.

Chua, E.F., Schacter, D.L., Rand-Giovannetti, E., and Sperling, R.A. (2007). Evidence for a specific role of the anterior hippocampal region in successful associative encoding. Hippocampus *17*, 1071-1080.

Collin, S.H., Milivojevic, B., and Doeller, C.F. (2015). Memory hierarchies map onto the hippocampal long axis in humans. Nat Neurosci *18*, 1562-1564.

Cooper, R.A., and Ritchey, M. (2019). Cortico-hippocampal network connections support the multidimensional quality of episodic memory. Elife *8*.

Cuellar, J.M., Alataris, K., Walker, A., Yeomans, D.C., and Antognini, J.F. (2013). Effect of high-frequency alternating current on spinal afferent nociceptive transmission. Neuromodulation *16*, 318-327; discussion 327.

Deans, J.K., Powell, A.D., and Jefferys, J.G. (2007). Sensitivity of coherent oscillations in rat hippocampus to AC electric fields. J Physiol *583*, 555-565.

Deng, Z.D., Lisanby, S.H., and Peterchev, A.V. (2013). Electric field depth-focality tradeoff in transcranial magnetic stimulation: simulation comparison of 50 coil designs. Brain Stimul *6*, 1-13.

Driver, J., Blankenburg, F., Bestmann, S., Vanduffel, W., and Ruff, C.C. (2009). Concurrent brain-stimulation and neuroimaging for studies of cognition. Trends Cogn Sci *13*, 319-327.

Eichenbaum, H. (2017). Prefrontal-hippocampal interactions in episodic memory. Nat Rev Neurosci *18*, 547-558.

Ekstrom, A.D. (2021). Regional variation in neurovascular coupling and why we still lack a Rosetta Stone. Philos Trans R Soc Lond B Biol Sci *376*, 20190634.

Eldridge, L.L., Engel, S.A., Zeineh, M.M., Bookheimer, S.Y., and Knowlton, B.J. (2005). A dissociation of encoding and retrieval processes in the human hippocampus. J Neurosci *25*, 3280-3286.

Esmaeilpour, Z., Jackson, M., Kronberg, G., Zhang, T., Esteller, R., Hershey, B., and Bikson, M. (2020). Limited Sensitivity of Hippocampal Synaptic Function or Network Oscillations to Unmodulated Kilohertz Electric Fields. eNeuro *7*.

Finn, B. (2017). A Framework of Episodic Updating: An Account of Memory Updating After Retrieval. Psychology of Learning and Motivation *67*, 173-211.

Fischl, B. (2012). FreeSurfer. Neuroimage *62*, 774-781.

Franke, M., Bhadra, N., Bhadra, N., and Kilgore, K. (2014). Direct current contamination of kilohertz frequency alternating current waveforms. J Neurosci Methods *232*, 74-83.

Goyal, A., Miller, J., Qasim, S.E., Watrous, A.J., Zhang, H., Stein, J.M., Inman, C.S., Gross, R.E., Willie, J.T., Lega, B.*, et al.* (2020). Functionally distinct high and low theta oscillations in the human hippocampus. Nat Commun *11*, 2469.

Gravitz, L. (2011). Drugs: a tangled web of targets. Nature *475*, S9-11.

Greenberg, B.D., Gabriels, L.A., Malone, D.A., Jr., Rezai, A.R., Friehs, G.M., Okun, M.S., Shapira, N.A., Foote, K.D., Cosyns, P.R., Kubu, C.S.*, et al.* (2010). Deep brain stimulation of the ventral internal capsule/ventral striatum for obsessive-compulsive disorder: worldwide experience. Mol Psychiatry *15*, 64-79.

Greinacher, R., Buhot, L., Moller, L., and Learmonth, G. (2019). The time course of ineffective sham-blinding during low-intensity (1 mA) transcranial direct current stimulation. Eur J Neurosci *50*, 3380-3388.

Grossman, N., Bono, D., Dedic, N., Kodandaramaiah, S.B., Rudenko, A., Suk, H.J., Cassara, A.M., Neufeld, E., Kuster, N., Tsai, L.H.*, et al.* (2017). Noninvasive Deep Brain Stimulation via Temporally Interfering Electric Fields. Cell *169*, 1029-1041 e1016.

Halgren, E. (1991). Firing of human hippocampal units in relation to voluntary movements. Hippocampus *1*, 153-161.

Hallett, M. (2007). Transcranial magnetic stimulation: a primer. Neuron *55*, 187-199.

Harmsen, I.E., Lee, D.J., Dallapiazza, R.F., De Vloo, P., Chen, R., Fasano, A., Kalia, S.K., Hodaie, M., and Lozano, A.M. (2019). Ultra-high-frequency deep brain stimulation at 10,000 Hz improves motor function. Mov Disord *34*, 146-148.

Hasgall, P.A., Di Gennaro, F., Baumgartner, C., Neufeld, E., Lloyd, B., Gosselin, M.C., Payne, D., Klingenböck, A., and Kuster, N. (2018). IT'IS Database for thermal and electromagnetic parameters of biological tissues.

Helbing, C., and Angenstein, F. (2020). Frequency-dependent electrical stimulation of fimbria-fornix preferentially affects the mesolimbic dopamine system or prefrontal cortex. Brain Stimul *13*, 753-764.

Herweg, N.A., Solomon, E.A., and Kahana, M.J. (2020). Theta Oscillations in Human Memory. Trends Cogn Sci *24*, 208-227.

Hothorn, T., Hornik, K., van de Wiel, M.A., and Zeileis, A. (2008). Implementing a Class of Permutation Tests: The coin Package. Journal of Statistical Software *28*, 1 - 23.

Huang, Y., and Parra, L.C. (2019). Can transcranial electric stimulation with multiple electrodes reach deep targets? Brain Stimul *12*, 30-40.

Iacono, M.I., Neufeld, E., Akinnagbe, E., Bower, K., Wolf, J., Vogiatzis Oikonomidis, I., Sharma, D., Lloyd, B., Wilm, B.J., Wyss, M.*, et al.* (2015). MIDA: A Multimodal Imaging-Based Detailed Anatomical Model of the Human Head and Neck. PLoS One *10*, e0124126.

Iglesias, J.E., Augustinack, J.C., Nguyen, K., Player, C.M., Player, A., Wright, M., Roy, N., Frosch, M.P., McKee, A.C., Wald, L.L.*, et al.* (2015). A computational atlas of the hippocampal formation using ex vivo, ultra-high resolution MRI: Application to adaptive segmentation of in vivo MRI. Neuroimage *115*, 117-137.

James, W. (1892). Psychology: Briefer Course (London: MACMILLAN AND CO).

Jenkinson, M., Bannister, P., Brady, M., and Smith, S. (2002). Improved optimization for the robust and accurate linear registration and motion correction of brain images. Neuroimage *17*, 825-841.

Jenkinson, M., Beckmann, C.F., Behrens, T.E., Woolrich, M.W., and Smith, S.M. (2012). Fsl. Neuroimage *62*, 782-790.

Johnson, L., Alekseichuk, I., Krieg, J., Doyle, A., Yu, Y., Vitek, J., Johnson, M., and Opitz, A. (2020). Dose-dependent effects of transcranial alternating current stimulation on spike timing in awake nonhuman primates. Sci Adv *6*.

Khadka, N., Harmsen, I.E., Lozano, A.M., and Bikson, M. (2020). Bio-Heat Model of Kilohertz-Frequency Deep Brain Stimulation Increases Brain Tissue Temperature. Neuromodulation *23*, 489-495.

Kilgore, K.L., and Bhadra, N. (2014). Reversible nerve conduction block using kilohertz frequency alternating current. Neuromodulation *17*, 242-254; discussion 254-245.

Korotkova, T., Ponomarenko, A., Monaghan, C.K., Poulter, S.L., Cacucci, F., Wills, T., Hasselmo, M.E., and Lever, C. (2018). Reconciling the different faces of hippocampal theta: The role of theta oscillations in cognitive, emotional and innate behaviors. Neurosci Biobehav Rev *85*, 65-80.

Krause, M.R., Vieira, P.G., Csorba, B.A., Pilly, P.K., and Pack, C.C. (2019). Transcranial alternating current stimulation entrains single-neuron activity in the primate brain. Proc Natl Acad Sci U S A *116*, 5747-5755.

Kuhn, J., Hardenacke, K., Lenartz, D., Gruendler, T., Ullsperger, M., Bartsch, C., Mai, J.K., Zilles, K., Bauer, A., Matusch, A.*, et al.* (2015). Deep brain stimulation of the nucleus basalis of Meynert in Alzheimer's dementia. Mol Psychiatry *20*, 353-360.

Kuznetsova, A., Brockhoff, P.B., and Christensen, R.H.B. (2017). lmerTest Package: Tests in Linear Mixed Effects Models. 2017 *82*, 26.

Lee, S., Lee, C., Park, J., and Im, C.H. (2020). Individually customized transcranial temporal interference stimulation for focused modulation of deep brain structures: a simulation study with different head models. Sci Rep *10*, 11730.

Lefaucheur, J.P., Andre-Obadia, N., Antal, A., Ayache, S.S., Baeken, C., Benninger, D.H., Cantello, R.M., Cincotta, M., de Carvalho, M., De Ridder, D.*, et al.* (2014). Evidence-based guidelines on the therapeutic use of repetitive transcranial magnetic stimulation (rTMS). Clin Neurophysiol *125*, 2150-2206.

Li, L.M., Violante, I.R., Leech, R., Ross, E., Hampshire, A., Opitz, A., Rothwell, J.C., Carmichael, D.W., and Sharp, D.J. (2019). Brain state and polarity dependent modulation of brain networks by transcranial direct current stimulation. Hum Brain Mapp *40*, 904-915.

Libby, L.A., Ekstrom, A.D., Ragland, J.D., and Ranganath, C. (2012). Differential connectivity of perirhinal and parahippocampal cortices within human hippocampal subregions revealed by high-resolution functional imaging. J Neurosci *32*, 6550-6560.

Lo, S., and Andrews, S. (2015). To transform or not to transform: using generalized linear mixed models to analyse reaction time data. Front Psychol *6*, 1171.

Lozano, A.M., Fosdick, L., Chakravarty, M.M., Leoutsakos, J.M., Munro, C., Oh, E., Drake, K.E., Lyman, C.H., Rosenberg, P.B., Anderson, W.S.*, et al.* (2016). A Phase II Study of Fornix Deep Brain Stimulation in Mild Alzheimer's Disease. J Alzheimers Dis *54*, 777-787.

Ma, D.S., Correll, J., and Wittenbrink, B. (2015). The Chicago face database: A free stimulus set of faces and norming data. Behav Res Methods *47*, 1122-1135.

Matsumoto, H., and Ugawa, Y. (2017). Adverse events of tDCS and tACS: A review. Clin Neurophysiol Pract *2*, 19-25.

Mayberg, H.S., Lozano, A.M., Voon, V., McNeely, H.E., Seminowicz, D., Hamani, C., Schwalb, J.M., and Kennedy, S.H. (2005). Deep brain stimulation for treatment-resistant depression. Neuron *45*, 651-660.

McCann, H., Pisano, G., and Beltrachini, L. (2019). Variation in Reported Human Head Tissue Electrical Conductivity Values. Brain Topogr *32*, 825-858.

McIntyre, C.C., and Grill, W.M. (1999). Excitation of central nervous system neurons by nonuniform electric fields. Biophys J *76*, 878-888.

McLaren, D.G., Ries, M.L., Xu, G., and Johnson, S.C. (2012). A generalized form of context-dependent psychophysiological interactions (gPPI): a comparison to standard approaches. Neuroimage *61*, 1277-1286.

Mukamel, R., Ekstrom, A.D., Kaplan, J., Iacoboni, M., and Fried, I. (2010). Single-neuron responses in humans during execution and observation of actions. Curr Biol *20*, 750-756.

Nielsen, J.D., Madsen, K.H., Puonti, O., Siebner, H.R., Bauer, C., Madsen, C.G., Saturnino, G.B., and Thielscher, A. (2018). Automatic skull segmentation from MR images for realistic volume conductor models of the head: Assessment of the state-of-the-art. Neuroimage *174*, 587-598.

Nitsche, M.A., and Paulus, W. (2011). Transcranial direct current stimulation--update 2011. Restor Neurol Neurosci *29*, 463-492.

O'Brien, P.L., Thomas, C.P., Hodgkin, D., Levit, K.R., and Mark, T.L. (2014). The diminished pipeline for medications to treat mental health and substance use disorders. Psychiatr Serv *65*, 1433-1438.

O'Connell, N.E., Cossar, J., Marston, L., Wand, B.M., Bunce, D., Moseley, G.L., and De Souza, L.H. (2012). Rethinking clinical trials of transcranial direct current stimulation: participant and assessor blinding is inadequate at intensities of 2mA. PLoS One *7*, e47514.

Opitz, A., Falchier, A., Yan, C.G., Yeagle, E.M., Linn, G.S., Megevand, P., Thielscher, A., Deborah, A.R., Milham, M.P., Mehta, A.D*., et al.* (2016). Spatiotemporal structure of intracranial electric fields induced by transcranial electric stimulation in humans and nonhuman primates. Sci Rep *6*, 31236.

Pikov, V. (2015). 18 - Global market for implanted neuroprostheses. In Implantable Neuroprostheses for Restoring Function, K. Kilgore, ed. (Woodhead Publishing), pp. 383-394.

Power, J.D., Barnes, K.A., Snyder, A.Z., Schlaggar, B.L., and Petersen, S.E. (2012). Spurious but systematic correlations in functional connectivity MRI networks arise from subject motion. Neuroimage *59*, 2142-2154.

Raco, V., Bauer, R., Olenik, M., Brkic, D., and Gharabaghi, A. (2014). Neurosensory effects of transcranial alternating current stimulation. Brain Stimul *7*, 823-831.

Raghavachari, S., Kahana, M.J., Rizzuto, D.S., Caplan, J.B., Kirschen, M.P., Bourgeois, B., Madsen, J.R., and Lisman, J.E. (2001). Gating of human theta oscillations by a working memory task. J Neurosci *21*, 3175-3183.

Rampersad, S., Roig-Solvas, B., Yarossi, M., Kulkarni, P.P., Santarnecchi, E., Dorval, A.D., and Brooks, D.H. (2019). Prospects for transcranial temporal interference stimulation in humans: A computational study. Neuroimage *202*, 116124.

Ranck, J.B., Jr. (1975). Which elements are excited in electrical stimulation of mammalian central nervous system: a review. Brain Res *98*, 417-440.

Ranganath, C., and Ritchey, M. (2012). Two cortical systems for memory-guided behaviour. Nat Rev Neurosci *13*, 713-726.

Riemann, S., Helbing, C., and Angenstein, F. (2017). From unspecific to adjusted, how the BOLD response in the rat hippocampus develops during consecutive stimulations. J Cereb Blood Flow Metab *37*, 590-604.

Ritchey, M., Libby, L.A., and Ranganath, C. (2015a). Cortico-hippocampal systems involved in memory and cognition: the PMAT framework. Prog Brain Res *219*, 45-64.

Ritchey, M., Montchal, M.E., Yonelinas, A.P., and Ranganath, C. (2015b). Delay-dependent contributions of medial temporal lobe regions to episodic memory retrieval. Elife *4*.

Ritchey, M., Yonelinas, A.P., and Ranganath, C. (2014). Functional connectivity relationships predict similarities in task activation and pattern information during associative memory encoding. J Cogn Neurosci *26*, 1085-1099.

Scangos, K.W., Khambhati, A.N., Daly, P.M., Makhoul, G.S., Sugrue, L.P., Zamanian, H., Liu, T.X., Rao, V.R., Sellers, K.K., Dawes, H.E.*, et al.* (2021). Closed-loop neuromodulation in an individual with treatment-resistant depression. Nat Med *27*, 1696-1700.

Schridde, U., Khubchandani, M., Motelow, J.E., Sanganahalli, B.G., Hyder, F., and Blumenfeld, H. (2008). Negative BOLD with large increases in neuronal activity. Cereb Cortex *18*, 1814-1827.

Shaw, K., Bell, L., Boyd, K., Grijseels, D.M., Clarke, D., Bonnar, O., Crombag, H.S., and Hall, C.N. (2021). Neurovascular coupling and oxygenation are decreased in hippocampus compared to neocortex because of microvascular differences. Nat Commun *12*, 3190.

Silberberg, D., Anand, N.P., Michels, K., and Kalaria, R.N. (2015). Brain and other nervous system disorders across the lifespan - global challenges and opportunities. Nature *527*, S151-154.

Small, S.A., Schobel, S.A., Buxton, R.B., Witter, M.P., and Barnes, C.A. (2011). A pathophysiological framework of hippocampal dysfunction in ageing and disease. Nat Rev Neurosci *12*, 585-601.

Smith, S.M. (2002). Fast robust automated brain extraction. Hum Brain Mapp *17*, 143-155.

Smith, S.M. (2004). Overview of fMRI analysis. Br J Radiol *77 Spec No 2*, S167-175.

Sperling, R., Chua, E., Cocchiarella, A., Rand-Giovannetti, E., Poldrack, R., Schacter, D.L., and Albert, M. (2003). Putting names to faces: successful encoding of associative memories activates the anterior hippocampal formation. Neuroimage *20*, 1400-1410.

Staudigl, T., and Hanslmayr, S. (2013). Theta oscillations at encoding mediate the context-dependent nature of human episodic memory. Curr Biol *23*, 1101-1106.

Strange, B.A., Witter, M.P., Lein, E.S., and Moser, E.I. (2014). Functional organization of the hippocampal longitudinal axis. Nat Rev Neurosci *15*, 655-669.

Sunshine, M.D., Cassara, A.M., Neufeld, E., Grossman, N., Mareci, T.H., Otto, K.J., Boyden, E.S., and Fuller, D.D. (2021). Restoration of breathing after opioid overdose and spinal cord injury using temporal interference stimulation. Commun Biol *4*, 107.

Thielscher, A., Antunes, A., and Saturnino, G.B. (2015). Field modeling for transcranial magnetic stimulation: A useful tool to understand the physiological effects of TMS? Annu Int Conf IEEE Eng Med Biol Soc *2015*, 222-225.

Vanderwolf, C.H. (1969). Hippocampal electrical activity and voluntary movement in the rat. Electroencephalography and Clinical Neurophysiology *26*, 407-418.

Venables, W.N., and Ripley, B.D. (2002). Modern Applied Statistics with S, Fourth edn (New York: Springer).

von Conta, J., Kasten, F.H., Curcic-Blake, B., Aleman, A., Thielscher, A., and Herrmann, C.S. (2021). Interindividual variability of electric fields during transcranial temporal interference stimulation (tTIS). Sci Rep *11*, 20357.

Whishaw, I.Q., and Vanderwolf, C.H. (1973). Hippocampal EEG and behavior: Change in amplitude and frequency of RSA (Theta rhythm) associated with spontaneous and learned movement patterns in rats and cats. Behavioral Biology *8*, 461-484.

Wicks, R.T., Witcher, M.R., Couture, D.E., Laxton, A.W., Popli, G., Whitlow, C.T., Fetterhoff, D., Dakos, A.S., Roeder, B.M., Deadwyler, S.A.*, et al.* (2020). Hippocampal CA1 and CA3 neural recording in the human brain: validation of depth electrode placement through high-resolution imaging and electrophysiology. Neurosurg Focus *49*, E5.

Wolodzko, T. (2020). Kernelboot: Smoothed bootstrap and random generation from kernel densities. R package version 0 *1*.

Woolrich, M.W., Behrens, T.E., Beckmann, C.F., Jenkinson, M., and Smith, S.M. (2004). Multilevel linear modelling for FMRI group analysis using Bayesian inference. Neuroimage *21*, 1732-1747.

Zeineh, M.M., Engel, S.A., Thompson, P.M., and Bookheimer, S.Y. (2003). Dynamics of the hippocampus during encoding and retrieval of face-name pairs. Science *299*, 577-580.

Figures and Legends

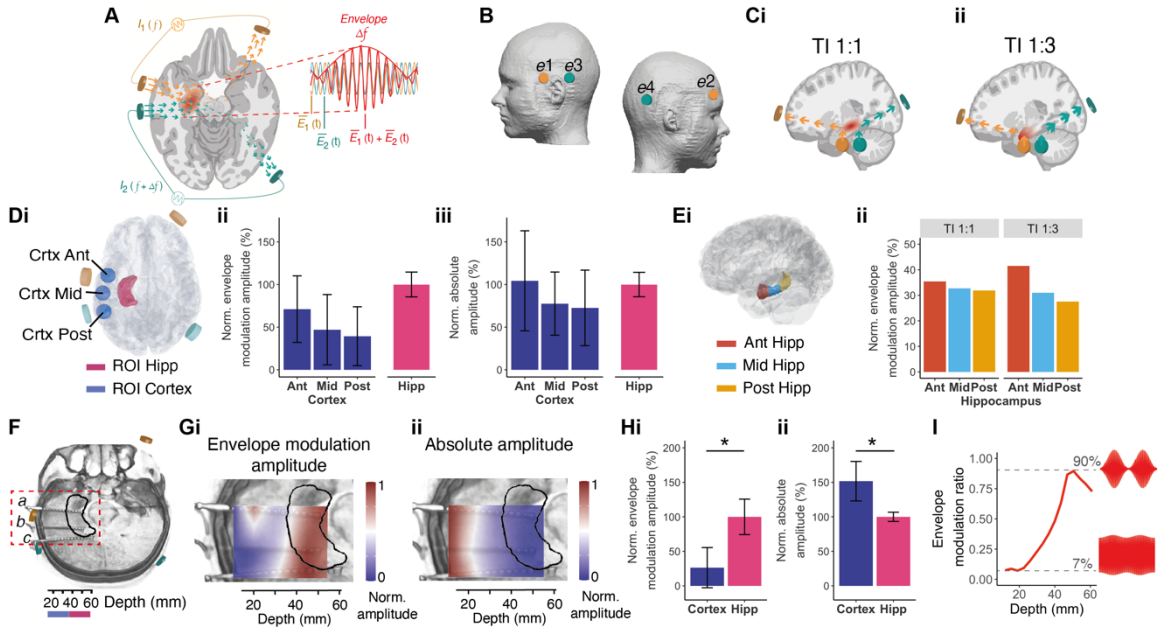

Figure 1. Fundamentals of Temporal Interference (TI) Hippocampal Stimulation and Validation Using Computational Modelling and Cadaver Measurements.

A-C Concept of transcranial TI hippocampal stimulation.

A. Two current sources I_1 and I_2 are applied simultaneously via electrically isolated pairs of scalp electrodes (orange and green) at kHz frequencies *f*1 and *f*2, with a small frequency difference Δf = *f*1- *f*2 within the range of neural activity. The applied currents generate oscillating electric fields $\bar{E}_1(t)$ and $\bar{E}_2(t)$ inside the brain (orange and green arrows, respectively). Superposition of these fields, $\bar{E}_1(t) + \bar{E}_2(t)$, results in an envelope amplitude that is modulated periodically at Δf. The peak amplitude of the envelope modulation can be localised in deep brain structures such as the hippocampus (highlighted in red).

B. Schematic of electrode configuration targeting the left hippocampus displayed in the standard head model. Electrodes *e*1 and *e*2 formed one electrode pair (orange) and electrodes *e*2 and *e*4 a second electrode pair (green), corresponding to current sources I_1 and I_2 in A. Electrodes *e*1 and *e*3 at the narrow base of the trapezoid were located at nasion plane of the left hemisphere, symmetrically above the anterior-posterior midline of the hippocampus, with a 5 cm distance between the electrode centres. Electrodes *e*2 and *e*4 at the wider base of the trapezoid were located at a plane above the eyebrow on the right hemisphere with approximately 16 cm distance between the electrode centres. All electrodes were 1.5 cm x 1.5 cm square with rounded corners.

C. Illustration how tuning the current ratios steers the TI stimulation locus along the hippocampal longitudinal axis. (i) TI stimulation with 1:1 current ratio ('TI 1:1') and stimulation locus in the middle region (ii) TI stimulation with 1:3 current ratio ('TI 1:3') and locus in the anterior region.

D-E Computation of TI stimulation locus in a human anatomical model.

D. Fields in regions of interest (ROIs) in the left (stimulated) hippocampus and its overlying cortex, showing **(i)** schematic of the regions of interest (ROIs); Ant – anterior, Mid – middle, Post – posterior. **(ii)** Fields' envelope modulation amplitude in the ROIs shown in (i), **(iii)** same as (ii) but for fields' absolute amplitude; shown values are median±SD normalised to the hippocampal value.

E. Envelope modulation amplitude in hippocampal ROIs. **(i)** Schematic of the Ant, Mid and Post ROIs along the hippocampal longitudinal axis, **(ii)** envelope modulation amplitudes in the

ROIs shown (i) during TI 1:1 and TI 1:3 stimulations; ROI amplitudes were normalised to total hippocampal exposure.

F-I. Measurement of TI stimulation locus in a human cadaver with I_1 (2 kHz, 1mA) and I_2 (2.005 kHz, 1mA).

F. CT image of the human cadaver with intracranial electrode leads *a*, *b* and *c* implanted in the left mesial temporal lobe. Each electrode consisted of 15 electrode contacts; Black contour, approximate location of the left hippocampus; orange and green stimulation electrodes.

G. Interpolated normalised amplitude map in the boxed region in **F** showing (i) envelope modulation amplitude map and (ii) absolute amplitude; See **Figure S1** for computation with conventional 5 Hz tACS.

H. Amplitudes in the left (stimulated) hippocampus and its overlying cortex **(i)** amplitude of envelope modulation showing peak at the hippocampus (**ii**) absolute amplitude showing peak in the overlying cortex; shown values are median±SD averaged across electrodes *a*-*c* and then normalised to hippocampal value. *p<0.05, See **Table S1** for full statistics.

I. Envelope modulation ratio vs depth for electrode *b*, showing increasing envelope modulation with depth.

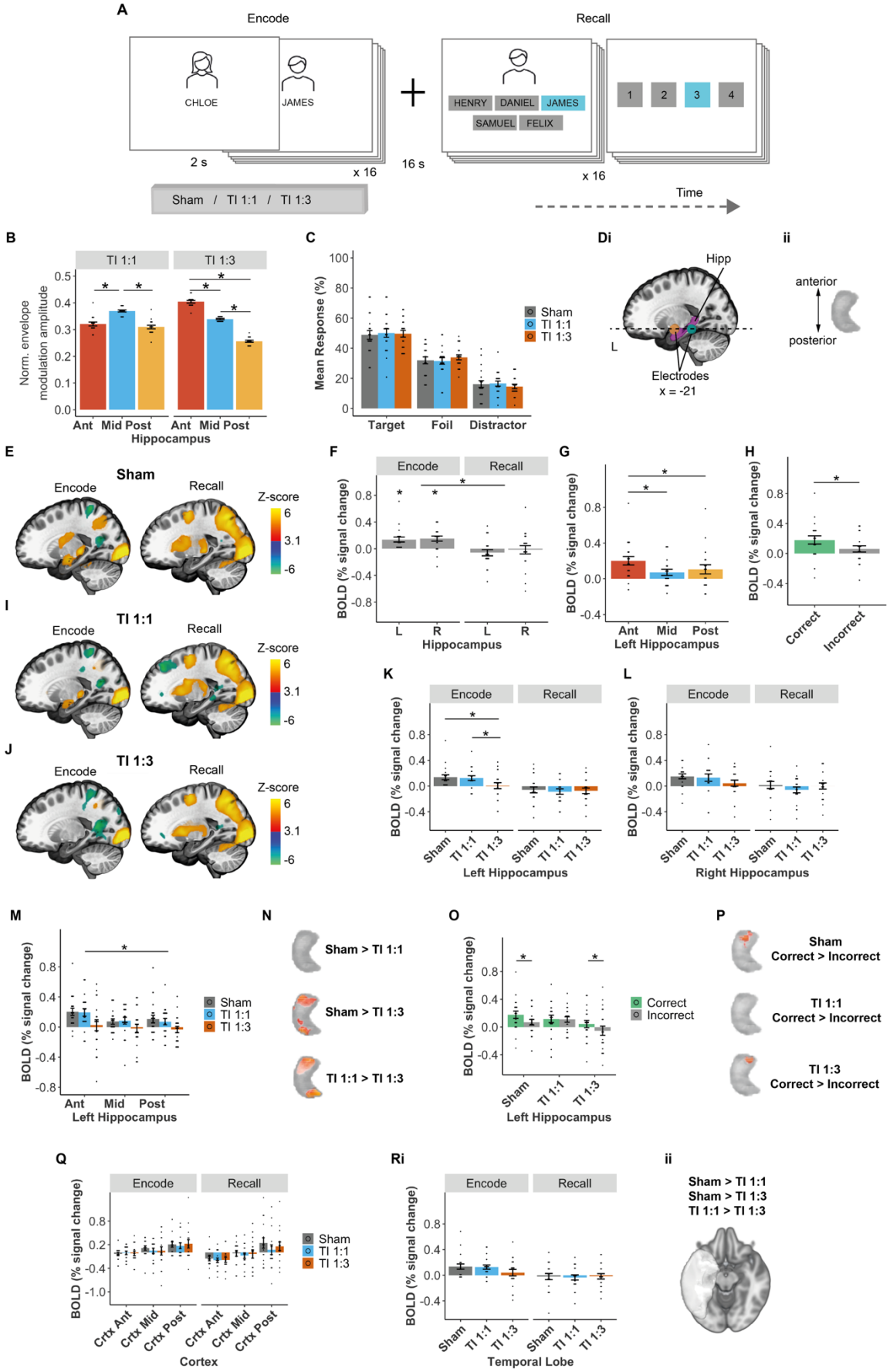

Figure 2. Probing the Physiological Effect of TI stimulation on Hippocampal Episodic Memory Activity.

A. Experimental Design for Hippocampal Dependent Face-Name Memory Task (the real stimuli used faces from the Chicago Face Database v.2.0.3, Ma et al., 2015).

B. Participants' envelope modulation amplitude in hippocampal ROIs shown in Figure 1Ei during TI 1:1 and TI 1:3 stimulations), computed with individualised MRI-based anatomical models; N=16 subjects; see Figure 1Ei for ROIs schematic. Showing a steering of the envelope amplitude peak from Mid hippocampal ROI during TI 1:1 stimulation to Ant hippocampal ROI during TI 1:3 stimulation; ROI amplitudes were normalised to total hippocampal exposure, see **Table S4** for full statistics.

C. Comparison of participants' memory performance across stimulation conditions showing a consistent higher recall rate of correct associations followed by foils and distractors. See **Table S5** for full statistics and **Figure S3** for additional performance metrics.

D. Anatomical location of the left hippocampus. **(i)** Sagittal plane view showing the location of the left hippocampus (Hipp; pink) and the relative position of stimulating electrodes in the left hemisphere (orange and green); displayed x = -21 of the MNI template. (**ii**) Axial plane view of the left hippocampus showing the anterior-posterior orientation.

E. Whole-brain group z-score change in BOLD signal during encode and recall stages of the task, showing a BOLD signal increase in the left hippocampus during the encoding, but not recall.

F. Group median change in BOLD signal in the left (L) and right (R) hippocampi during encoding and recall stages in sham condition blocks. Showing significant BOLD signal increase during the encode, but not recall stage; see **Table S6** for full statistics.

G. Group median change in BOLD signal in the anterior (Ant), middle (Mid) and posterior (Post) regions of the left hippocampus during the encoding stage in the sham condition; see Figure 1Ei for ROIs schematic. Showing a larger BOLD signal increase in the Ant hippocampal region in relation to the Mid and Post regions; see **Table S7** for full statistics.

H. Group median change in BOLD signal in the left hippocampus for memory associations encoded correctly (green) and incorrectly (grey). Showing significantly higher BOLD signal for correct compared to incorrect associations, see **Table S8** for full statistics.

I-J. Same as **(E)** but for the TI 1:1 (**I**) and TI 1:3 (**J**) stimulation conditions. Note the increase in BOLD signal in the left hippocampus during encode for the TI 1:1 condition, similar to sham (**E**), but not for the TI 1:3 condition.

K. Comparison of group median change in BOLD signal between stimulation conditions, in the left (i.e. stimulated hippocampus) during encoding and recall stages. Showing an effect of stimulation and reduction in the evoked BOLD signal in the left hippocampus during encoding stage by TI 1:3 stimulation; see **Table S9** for full statistics.

L. Same as (**K**) but for the right hippocampus, where there is no effect of stimulation; see **Table S9** for full statistics.

M. Comparison of group median change in BOLD signal between stimulation conditions, in the Ant, Mid, and Post regions of the left hippocampus during the encoding stage; see Figure 1Ei for ROIs schematic. Asterisk indicates a reduction in the evoked BOLD signal during the TI 1:3 stimulation across regions; see **Table S11** for full statistics.

N. Voxelwise group-level contrasts comparing stimulation conditions in the left hippocampus, confirming higher BOLD signal for the sham and TI 1:1 conditions compared to the TI 1:3 condition. No significant voxels observed for the comparison between sham and TI 1:1, confirming the results observed in the hippocampal ROIs.

O. Same as (**H**) but for all stimulation conditions. Showing significantly higher BOLD signal for correct compared to incorrect associations in the left hippocampus during sham and TI 1:3, see **Figure S4** and **Table S11** for full statistics.

P. Voxelwise group-level contrasts comparing correct and incorrect encoded associations in the left hippocampus, showing that BOLD signal during the formation of correct associations is predominantly modulated in a cluster located in the anterior portion of the hippocampus for sham and TI 1:3 conditions, while no differences between BOLD signal for correct and incorrect associations were observed for the TI 1:1 condition.

Q. Comparison of group median percentage change in BOLD signal between stimulation conditions, in the anterior (Ant), Middle (Mid), and posterior (Post) regions of the overlying cortex; see Figure 1Di for ROIs schematic; see **Table S12** for full statistics. Showing no difference in the BOLD signal change between stimulation conditions.
R. Comparison of BOLD signal between stimulation conditions in the left temporal lobe (excluding the hippocampus), (**i**) median change in BOLD signal, (**ii**) voxelwise group-level contrasts; both showing no significant differences between stimulation conditions.
Asterisks identify significant differences, p<0.05. Bar plots show mean and standard error (SE), black dots show individual participant data. E-J images were thresholded at Z > 3.1, with a cluster significance level of p<0.05, and are displayed in x = -21 plane of the MNI template. N,P and Rii images were thresholded at significance level of p<0.05, voxelwise permutation-based t-tests on the ROI. N=20 throughout except for Q where N=16.

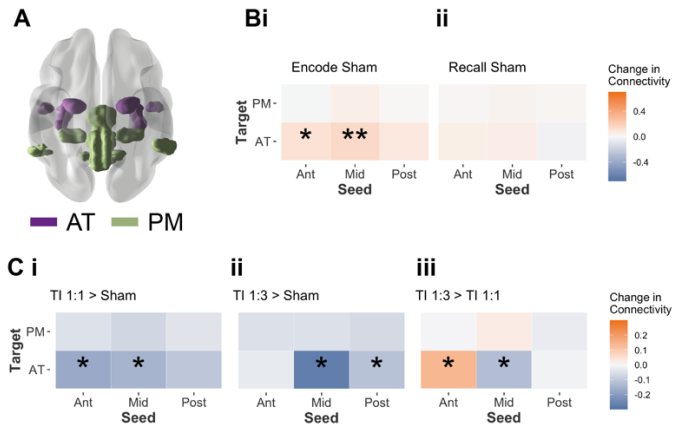

Figure 3. TI Stimulation Change in Hippocampal-Cortical Functional Connectivity During Face-Name Memory Task (Human Experiment 1).
A. Antero-temporal (AT, purple) and posterior-medial (PM, green) hippocampal-cortical networks.
B. Group mean change (% signal change) in functional connectivity between the anterior (Ant), Middle (Mid), and posterior (Post) regions of the left (L) hippocampus and the AT and PT networks during encoding and recall task stages in sham blocks (i.e., without stimulation) for the contrast correct > incorrect. Showing a larger connectivity between the Ant and Mid regions of the L hippocampus and the AT network during encoding of successful associations; one-sample t-tests; N=20; **, p < 0.05 FDR-corrected; *, p < 0.05 uncorrected; see **Table S14** for full statistics.
C. Effect of TI stimulation on functional connectivity, showing the same as B but comparing changes between stimulation conditions during encoding stage in which a connectivity increase was observed in sham blocks. (**i**) TI 1:3 compared to sham, (**ii**) TI 1:1 compared to sham, (**iii**) TI 1:3 compared to TI 1:1. Showing a reduction in functional connectivity by both TI 1:1 and TI 1:3 stimulations (relative to sham), and when comparing the TI stimulations, a larger connectivity in the Mid region during TI 1:1 and in the Ant region during TI 1:3 (LMM with significant 3-way interaction between stimulation type, seed and network; *, p < 0.05 corrected post-hoc contrasts; see **Table S14** for full statistics).

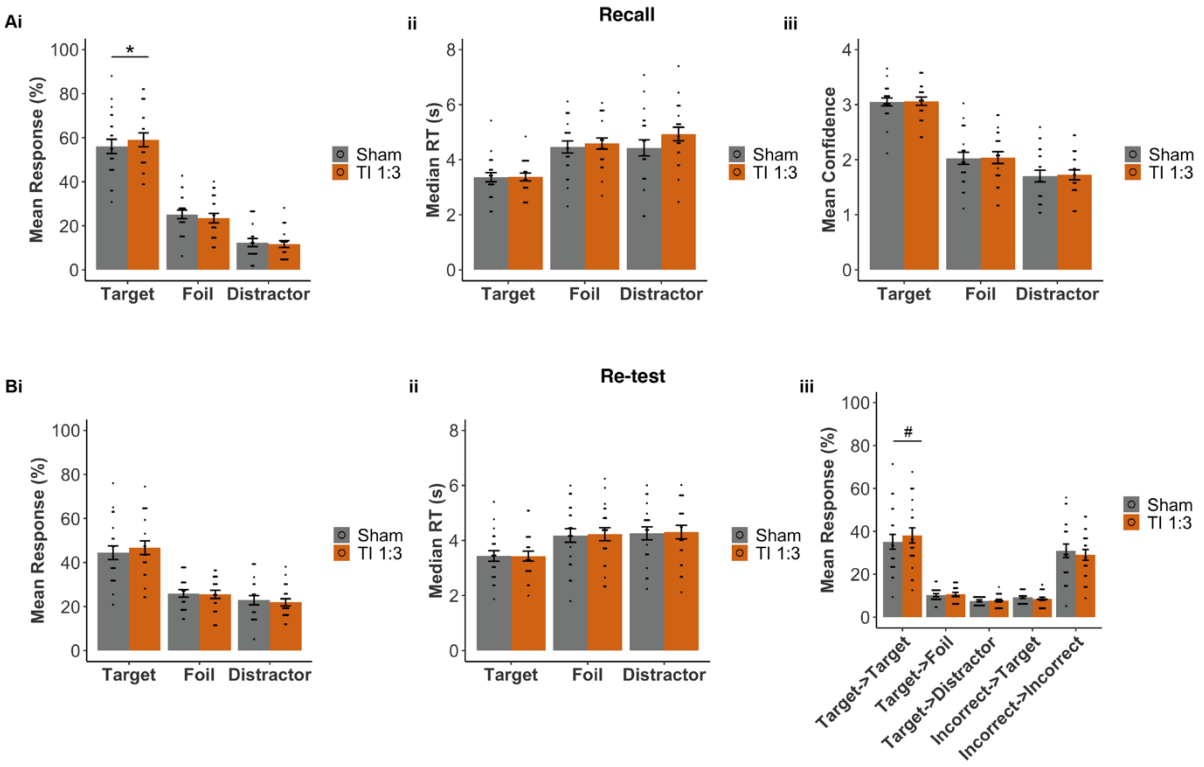

Figure 4. Probing the Effect of Hippocampal TI Stimulation on Behavioural Function.
A. Comparison of participants' memory performances during recall between sham (grey) and TI 1:3 (orange) across recall type (target, foil and distractor). (**i**) Percentage response, showing higher probability of target responses, i.e. face-name pairs correctly remembered. (**ii**) Median reaction time, showing no differences between stimulation conditions. (**iii**) Mean confidence ratings, which were also similar between stimulation conditions. See **Table S21** for full statistics.
B (i-ii). Same as (**Ci-ii**) but for re-test. (**iii**) Comparison between sham and TI 1:3 stimulation for the memory performance for each face-name pair. We assigned one of 5 categories to each face-name pair that summarise the outcome of each pair from recall to re-test: 1) Target -> Target are associations correctly identified in recall and re-test; 2,3) Target -> Foil/Distractor are associations correctly identified during recall, but forgotten during re-test, with participant selecting foil or distractor, respectively; 4) Incorrect -> Target are associations incorrectly remembered at recall, but correctly matched at re-test; 5) Incorrect -> Incorrect are associations incorrectly remembered at both recall and re-test. Cardinal (#) indicates significant exploratory post-hoc for Target ->Target condition, trend level main effect of stimulation. See **Table S22** for full statistics
Bar plots show mean and standard error (SE), black dots show individual participant data. Asterisks (*) indicate significant post-hoc comparisons between stimulation conditions.